

Response to Reviewer 1

August 26, 2019

Manuscript title: Reconstructing the Salgar 2015 Flash Flood Using Radar Retrievals and a Conceptual Modeling Framework: A Basis for a Better Flood Generating Mechanisms Discrimination

Authors: Nicolás Velásquez, Carlos D. Hoyos, Jaime I. Vélez, and Esneider Zapata

General Concept:

I already did the revision of the two first versions of manuscript. I really appreciate the supplementary information added in the manuscript, namely the figure 9, explaining the floodplain iterative assessment; the new discharge data, that comforts the hydrological model results, and the information concerning the stream velocity in Annexe.

However, I'm a bit upset that there are still a lot of annotation issues, and writing mistakes that might exist on the first submission but really not of the third one. Several co-authors comments are also spread within the text. Quick checks of the homogeneity and the consistency of the equations and annotations should be done before submitting and NOT by the reviewer. As example in the hydrological model, you mentioned calibrated parameters that are not in the equations of the model. Also the indexation of the variables/ parameters are still sporadic.

I'm convinced there is a lot of work behind the paper, and that each part of the modeling framework should have been a main topic on its own, making easier the writing, the results analysis and the reading. Nevertheless I respect the choice of the paper to gather the modeling work in one paper. In addition I would have personally chosen a slightly different way to highlight the results and to orientate the discussion on several points. But again you're the only ones to choose the direction of your paper.

I divided my comment in three parts. The first one consists in several modifications of the section 3 to make clearer the methodology description, specially the hydrological model and the floodplain submodel description. Those comments and/or suggested modifications are very important and almost unavoidable (from my point of view) to clarify and make the method understandable. In the second part, I made some comments and suggestions on the results and on the discussion that should make the paper insights be highlighted. And finally in the last part, I pointed out the spelling or language mistakes I found.

We sincerely thank again the reviewer. We are truly impressed by her careful, and detailed review. We feel truly lucky having had her as a reviewer of our work. We would also like to apologize for the writing mistakes, typos and for the poor description of the hydrological model. In hindsight, part of the issue is due to the fact that we were able to integrate most of the comments by both reviewers in the new versions, improving the manuscript, but we failed to integrate some of them in a proper way, leading to organization issues in the manuscript. We think we managed to do that in the current version of the manuscript. Also, we have rewritten the model and submodel formulations in detail, following the suggestions by the reviewer.

We understand the point about having considered at the beginning writing this work as two separate manuscripts, one on the modeling framework and other on the Salgar event, but as the reviewer mentioned, we wanted to have the modeling framework highlighted by a real and relevant

application.

We have taken in consideration all the suggestions, and we have modified the manuscript accordingly.

1 Comments on the sections

1.1 Comments on the methodology's description

Description of the hydrological model

- **Page 13, line 303-305:** I don't understand this sentence "Vertical flows are only time dependent, while lateral flows could also depend on the actual state of the tank (kinematic approximation)." The vertical flows also depend on the actual state of the tank, doesn't it? I would suggest to remove this sentence.

Yes, the reviewer is completely right. The vertical flows also depend on the state of the tank. The sentence was poorly worded. We have removed the sentence.

- **Page 13, lines 306-309:** You mentioned 4 modifications of the hydrological model but I don't agree with the fact to classify two of them as modification: The first one, "the direct use of radar QPE [...]" : it is not a modification, but it is a specific choice of rainfall inputs. The 4th modification: "the development of two modules [...]" : this refers to the "landslide submodel" and the "HydroFlash submodel". For my understanding, it is not a modification of the hydrological model, but additional modelling elements that use the results of the hydrological model. I'm sorry to be picky, but I think for an easy understanding of the paper, you should strictly follow the subsections's structure and only mention here what is related to the hydrological model.

The reviewer is right. Allowing the direct use of QPE rainfall is a technical modification and not a hydrological one. Also, the addition of a landslide and a floodplain submodels do not directly modified the equations of the TETIS model so it is not an actual modification of the model but of the modeling framework. We have modified the text following the summary suggestion by the reviewer.

- **Page 13, 311-317:** I prefer when this part was inserted in the results description. The cell classification is a tool to analyze the spatially heterogeneous response of the catchment. I would even suggest to merge the figure 7 and the figure 14, keeping only the 50 classes categorizations of the figure 7 used in the Figure 14. Moreover I don't understand the first sentence and the expression "soil-rainfall-discharge coupling holistically". Another option would be to introduce this in the same section as the virtual tracers.

We agree with the reviewer and we accept the suggestion. We merged again Figures 7 and 14, including only the example of the 50 groups. Also, in the description we modified the sentence **soil-rainfall-discharge coupling holistically to: Additionally, we propose a graphical method to analyze, at the same time, the evolution of multiple hydrological variables in the entire basin.** The description of the graphical method is included in the **Tools for spatial analysis of the results: virtual tracers and catchment cell grouping** subsection, and the figure and its description are included in the **Results** section.

- **Page 14, figure 6:** in the Hydrological modelling panel, the storage tanks are called "Ti", but the "Si" parameters are not mentioned as the legend does.

The reviewer is right; it was our mistake. The name of the variable in Figure 6 and in the equation is S_i and not T_i . We modified Figure 6 in order to match the equation.

- **Page 14, title section 3.1.1:** the modelling modifications are not only related to runoff but to all the lateral flow; I would suggest to call this section "Lateral flow modelling modifications"

We agree with the reviewer and have changed the title of the section to: **Lateral flow modeling modifications**.

- **Page 15 – 16:** the variable $A_i(t)$, called in the text “sectional area of the storage”, has actually no unit [-], according to the equation (6). Reading Velez’s thesis, it seems rather to be a coefficient. The actual sectional area is $S_i(t) * \Delta x$. This error makes the understanding of the equation really complex, and even makes me doubt about the meaning of the equation.

The description of the model was rewritten considering the reviewers suggestions and concerns. The text of the subsection is now written as follows:

The TETIS model relies on the concept of mass balance where the storage of tank i at the end of the simulation interval $S_i(t)^*$ [mm] is function of the storage at the start of the simulation interval $S_i(t)$ [mm] and the storage outflow $E_i(t)$ [mm] during the interval t , as follows:

$$S_i(t)^* = S_i(t) - E_i(t) \quad (1)$$

The storage outflow E_i is estimated by transforming the storage $S_i(t)$ into an equivalent cross sectional area A_i [m^2], as follows:

$$A_i(t) = S_i(t)F_c/\Delta x, \quad (2)$$

where Δx [m] is the model cell width, and F_c [$\text{m}^3 \text{ mm}^{-1}$] is a units conversion factor that is equal to the area of each cell element A_e [m^2] multiplied by 1 m/1000 mm. According to [34], E_i changes as a function of A_i , the flow speed v_i [ms^{-1}], and the model time step Δt [s], as follows:

$$E_i(t) = A_i(t)^*v_i(t)\Delta t/F_c. \quad (3)$$

The expression for the cross sectional area at the end of the simulation period $A_i(t)^*$ is found by replacing $S_i(t)$ in equation (2) for $S_i(t)^*$, and then resulting expression and equation (3) into equation (1),

$$A_i(t)^* = \frac{S_i(t)F_c}{\Delta x + v_i(t)\Delta t}. \quad (4)$$

Equation (4) is solved coupled with the equation for the speed v_i :

$$v_i(t) = \beta A_i(t)^\alpha \quad (5)$$

Equation 5 is the generic formulation for the speed used in this work to represent nonlinearities in the relationship between v_i and A_i . In the formulation, both, β and α change depending on the type of flow: overland, subsurface, base, and channel flow. The solution for v_i is obtained by using the successive substitution method described by [6]. In the model, we use a 5-minute time step which ensures the stability of the computations. When a solution is reached, E_i is computed using equation (3) and S_i is updated using equation (1).

Nonlinear equations in lateral flows result in a better representation of processes at high resolutions [4, 19]. A nonlinear approximation of runoff is presented in equation 6. This approximation is a modification of Manning’s formula for flow in gullies. According to [12], ε and e_1 are a coefficient and an exponent used to translate the Manning channel concept into multiple small channels or gullies. The values of ε and e_1 are 0.5 and 0.64, respectively [12]. $A_{i,2}$ [m^2] is the corresponding sectional area obtained from $S_{i,2}$ by using equation (4). In addition, $M_{i,0}$ is the slope of the cell, and n_i is the Manning coefficient.

$$v_{i,2} = C_7 \frac{\varepsilon}{n} M_{i,0}^{1/2} A_{i,2}(t)^{(2/3)e_1} \quad (6)$$

The nonlinear equation 7 corresponds to an adaptation of the [21] formula for subsurface runoff $v_{i,4}$, where $k_{i,s}$ is the saturated hydraulic conductivity of cell i , and the exponent b is dependent on the soil type, and it is assumed to be equal to 2. $A_{i,g}$ is the equivalent cross-section area of the maximum gravitational storage ($H_{i,g}$ [mm]). $A_{i,3}$ is the corresponding sectional area for the gravitational storage ($S_{i,3}$) obtained by using equation (4). There is also return flow from tank 3 to tank 2, when $S_{i,3} = H_{i,g}$, which represents runoff generation by saturation. In the case of the base-flow, we assume that the speed $v_{i,4}$ is constant for each cell and depends on the aquifer hydraulic conductivity $k_{i,p}$ (see equation 8).

$$v_{i,3} = C_8 \frac{k_{i,s} M_{i,0}^2}{(b+1) A_{i,g}^b} A_{i,3}(t)^b \quad (7)$$

$$v_{i,4} = C_9 k_{i,p} \quad (8)$$

Finally, the stream flow velocity is calculated by using the geomorphological kinematic wave approximation [34?], in which Λ [km²] represents the upstream area, and Ω and ω_i , a regional coefficient and regional exponents, respectively

$$v_{i,5} = C_{10} \Omega M_{i,0}^{\omega_1} \Lambda_i^{\omega_2} A_{i,5}^{\omega_3} \quad (9)$$

The streamflow speed expression is a version of equation (5). This considering that the terms Ω , $M_{i,0}^{\omega_1}$, Λ^{ω_2} , and the exponent ω_3 are constant with time.

- **Page 15:** definition of v_i : I'm not familiar with the dimensionless variable A_i you defined. I used to use relationship between velocity and hydraulic radius or storage water level.

See response to previous comment. The variable A_i [m²] refers to the equivalent equivalent cross sectional area of the tank i , as follows

- **Page 15-16, equations 1- 8:** I would suggest to present the general equations that control all the lateral flow first (eq. 7, 6, 1), before indicating the particularity of each tank lateral flow (eq. 2-5).

We agree with the reviewer. We have rewritten the section as shown in the responses to the previous two comments.

- **Page 15, line 334:** please call the slope in a different way, it might be confused with the tank levels S_i .

We modified the variable following the suggestion by the reviewer. The slope is now referred to as $M_{i,0}$.

- **Page16, equation 5:** how we are suppose to understand the equation? There is more exponents than parameters.. please also simplify, specially if at the end you will use a regional parameter deduce from any catchment.. Here what is important is the fact that v_5 is depending not only on A_5 but also on the stream bed slope. Only 3 parameters should appear : $v_5 = \beta * S_i(t)^\alpha S_0^\lambda$.

We thank the reviewer. There was a typo in equation. We have now corrected it. The correct form of the equation is: $v_{i,5} = C_{10} \Omega M_{i,0}^{\omega_1} \Lambda_i^{\omega_2} A_{i,5}^{\omega_3}$. In the formulation made by [34], the equation depends the slope $M_{i,0}$, the upstream area Λ_i [km²], and the equivalent sectional area $A_{i,5}$ [m²]. The parameters correspond the the coefficient Ω and the exponents ω_1 , ω_2 , and ω_3 . According to [34], the regional variables are constant for all the watershed. For each channel element, the equation can be rewritten by grouping in a single coefficient the terms β_c the

constant parameters Ω , $M_{i,0}^{\omega_1}$, and Λ^{ω_2} . This results in an equation that has the same form as the generic equation $v_{i,5} = \beta A_{i,5}(t)^{\omega_3}$. An extended discussion of the regional parameters can be found in [34].

- **Page 16, page 366-367:** Δx versus L : Actually according to Velez, 2011 page 89; the ΔX variable used his thesis correspond to the cell width; i.e. the resolution if the flow direction is orthogonal or $\Delta x\sqrt{2}$ if the flow direction is diagonal.

The reviewer is correct, in the model $L = \Delta X$ if the flow direction is orthogonal, and $L = \Delta x\sqrt{2}$ if the direction is diagonal. The text and the equations have been modified accordingly.

- **To summary the remarks I did from page 12, line 290 to page 16, line 372, I would suggest to reword more or less as follow:**

We used a physically-based and distributed model developed and described in Vélez (2001) and Frances et al. (2007). The spatial distribution and the hydrological flow path schema is based on the 12.75 m resolution DEM data. In each cell, five tanks represent the hydrological processes including capillary (tank 1), gravitational (tank 2), runoff (tank 3), baseflow (tank 4) and channel storage (tank 5). The state of each tank varies as a function of vertical and lateral flows as shown in the diagram, where the storage is represented by S_i [m] and the vertical input to each tank by D_i [m], which in turns depends on the vertical flow through tanks R_i [m]. E_i represents the downstream connection between cells, except for tank 1, where E_1 represents the evaporation rate.

The original model fully described in Vélez (2001) and Frances et al. (2007) are modified to improve the representation of the flow processes that occur during flash floods (see section 3.1.1). In addition, two analysis tools of the hydrological modelling results are introduced: virtual tracers tracking precipitation origins as well as water paths over or through the soils; and catchment cell grouping (see section 3.1.2). The tools objective is to allow an analysis of the spatially distributed response of the catchment.

We thank the reviewer for the careful review of the model equations. We have modified the text and the model formulation, being careful in the equation typewriting, the coherence between the text, the variables and the equations, the completeness of the model description, and considering all the suggestions made by the reviewer.

- **Page 17, line 396:** hydrological and not hydrologic.

We corrected the word in the entire document.

- **pages 17, line 410 – 412:** I would suggest to speak about the calibrated parameters rather than the non calibrated parameters.

We have change the text to list the parameters that were calibrated.

- **page 18, table 3:** the parameters you mentioned in the table are not in the related equations.

We have modified Table 3 to explicitly relate all the parameters to the model equations. Also, the caption of the table was modified to describe the parameters not included in the model formulation.

- **page 18, table 3:** Assuming the velocity parameters correspond of the velocity of each flow when the related water storage is equal to 1; I would expect the increasing magnitude order: Subterranean speed, subsurface speed, surface speed, channel speed. How can you explain that the subsurface speed is higher than all the other ones?

We believe that this might be a misunderstanding caused by the original description and setup of Table 3. In the new Table 3, it can be seen that the mentioned value corresponds to an scalar coefficient that multiplies the physical value of the velocities, rather than the actual physical value. In other words, the constants C_i corresponds to calibration coefficients: $v_i = C_i B_i A_i^\alpha$,

where C_i is the calibrating parameter, B_i the physical factor, A_i the corresponding sectional area, and α the exponent. To avoid misunderstandings, we deleted the **mean value** column.

On a side note, the reviewer is correct, in the model the mean speed of each tank increase from the subterranean storage to the runoff.

- **page 18, line 417:** please remove “above the slip surface $Z_{i,w}$ ”.

We appreciate the reviewer comment. We re-phrase the corresponding paragraph to: The landslide submodel coupled to the TETIS model is proposed by [1]. The stability of each cell is calculated through the assessment of the different stresses applied to the soil matrix. The coupling between TETIS and the landslide submodel is required because the stability of the soil decreases with the pore water pressure [17]. The saturated soil depth $Z_{i,w}$ depends on the gravitational storage $S_{i,3}(t)$, the soil wilting point $W_{i,pwp}$, and the soil field capacity $W_{i,fc}$, as follows:

$$Z_{i,w}(t) = \frac{S_{i,3}(t)}{W_{i,fc} - W_{i,pmp}} \quad (10)$$

- **page 19, line 441:** I suggest the following title “the floodplain submodel Hydroflash”.

Following the reviewer comment, we changed the title to: Floodplain submodel (Hydroflash)

- **page 21, line 477:** $A_{i,sed}$ meaning: Is really the flooded area (area along x,y) or the sectional area along the cross profile (area along z,y, x being the stream flow direction)? According to the attributed name, it seems to be the first definition; but according to the figure 9, I would say the second definition. It makes a big difference...

We agree with the reviewer, the text in its original form leads to misunderstandings. We have corrected the document, and, in addition, we now refer to $A_{i,load}$, as suggested by the reviewer.

- **page 19-20:** Hereafter I'll suggest some rewording, introducing ALL the annotations. The equation references has to be added. It is roughly drafted. Please, feel free to integrate or not.

[...]

We appreciate the reviewer's advice about the floodplain submodel description. In the new version of the document, we rewrote following all the comments by the reviewer, as follows:

The HydroFlash submodel is designed to interpret the TETIS simulations as floodplain inundations (Figure 8). For each stream cell and at each time step, the submodel (i) calculates the stream discharge including sediment load (equations 11 - 16, see [33]), and (ii) determines the inundated cells according to the stream cross-profile, the sectional area, and the stream velocities when including the sediment load (equations 15 - 17, [33]). To determine the discharge including sediment load ($Q_{i,load}$), a realistic channel width is calculated according to [22] approach as

$$W_i = 3.26Q_i^{-0.469} \quad (11)$$

where Q_i corresponds to the streamflow estimated based on a long-term water balance.

Assuming an infinite sediment and rubble supply, equations 12, 13, 14 are used to deduce, from the channel width W_i , the water level Y_i (equation (12)), the friction velocity $v_{i,fr}$ (equation (12, described in [33]), the sediment concentration c_i (equation (14)), and finally the sediment-loaded stream discharge (equation (16)), as follows:

$$Y_i(t) = \frac{Q_{i,sim}(t)}{v_{i,sim}(t)W_i} \quad (12)$$

$$v_{i,fr}(t) = \frac{v_{i,sim}(t)}{5.75 \log \left(\frac{Y_i(t)}{D_{i,50}} \right) + 6.25} \quad (13)$$

$$c_i(t) = C_{max} (0.06 Y_i(t))^{\frac{0.2}{v_{i,fr}(t)}} \quad (14)$$

$$r_i(t) = \frac{1}{D_{i,50}} \left[\frac{g}{0.0128} \left(c_i + (1 - c_i) \frac{\gamma_w}{\gamma_{sed}} \right) \right]^{1/2} \cdot \left[\left(\frac{C_{max}}{c_i} \right)^{1/3} - 1 \right] \quad (15)$$

$$Q_{i,load}(t) = \frac{Q_{i,sim}(t)}{1 - c_i(t)} \quad (16)$$

where $v_{i,sim}$ and $Q_{i,sim}$ are the simulated velocity and streamflow, respectively. Also, r_i is the constitutive coefficient of the flow, that summarizes the flow dynamics associated with sediments and colliding particles. The above mentioned relationships depend of 2 parameters: the maximum sediment concentration (C_{max} [-]) and the characteristic diameter of the sediments $D_{i,50}$ [m]. Both terms are assumed to be constant and equal to 0.75 [26] and 0.138 [16], respectively.

To determine the inundated cells, the flood depth ($F_{i,d}$) and the sectional area of the stream including sediments ($A_{i,load}$) are iteratively calculated by reducing the difference between $Q_{i,load}$ and $\hat{Q}_{i,load}$. The channel cross-section for cell i , $E_{i,bed}$, is defined by the DEM. In each iteration N , the model updates $F_{i,d}$ with a $\Delta y = 0.1$ m increase. The cross sectional area $A_{i,load}$ is calculated by taking difference between $F_{i,d}$ and the elevation of each cell j in the cross-section $E_{i,bed}$.

$$\hat{Q}_{i,load}(t) = 0.2 r_i(t) (N \Delta y)^{\frac{3}{2}} S_{i,0} A_{i,load}(t) \quad (17)$$

$$F_{d,i}^N = F_{d,i}^{N-1} + \Delta y \quad (18)$$

$$A_{i,load}^N = \Delta x \sum_{j=1}^N F_{i,j,d}^N - E_{i,j,bed} \text{ with } E_{i,j,bed} < F_{i,j,d}^N \quad (19)$$

The resulting flood maps might include the presence of small isolated flood spots and discontinuities where the flow direction changes from orthogonal to diagonal across or vice versa. We included two post-processing steps to correct these issues by (i) using an image processing erosion algorithm [32] to remove the small and isolated flood spots (step 4 in Figure 8), and, to solve the flow direction discontinuities, (ii) for each flooded cell the model seeks to inundate the eight neighboring cells: A neighbor cell is also flooded if the altitude of the original flooded cell, plus the flood depth, is higher than its elevation (step 5 in Figure 8). The image erosion is performed once with a 3 by 3 kernel. An example of the final result for a time step t is shown in the step 6 in Figure 8.

- **Page 19-20** about the HydroFlash model: I'm curious to know about the ratio Q_{sed}/Q_{sim} : what is the range of value of c ? Is there a significant change to include the sediments when calculating the floodplain?.

The simulated peak discharge Q_{sim} with the final parameterization used in the study is $220 \text{ m}^3 \text{s}^{-1}$, and the streamflow with the sediment load reached values around $285 \text{ m}^3 \text{s}^{-1}$, for a Q_{sed}/Q_{sim} ratio of 1.3. The extra 30% discharge is certainly a relevant contribution with impacts in the floodplain simulations. We added this comment in the discussion section, as follows.

Similarly, results of the HydroFlash submodel are satisfactory despite the hydraulic over simplifications, and are potentially useful for issuing warnings to the community. From that point

of view, it is important to stress that the low computing cost of HydroFlash, different to that of detailed 2D/3D hydraulic geomorphological models, makes it possible to be executed in real time coupled with rainfall observations, providing valuable information that, while not 100% accurate spatially, helps discriminating to a high degree, for example, which communities need to be evacuated given an extreme event. In addition, the floodplain submodel provides an indirect estimation of the sediment load during extreme events. In the 2015 Salgar simulations, the peak discharge obtained with the hydrological model was $220 \text{ m}^3\text{s}^{-1}$; the total streamflow considering the sediment load reached values around $285 \text{ m}^3\text{s}^{-1}$, for a $Q_{\text{sed}}/Q_{\text{sim}}$ ratio of 1.3. The extra 30% discharge corresponding to the sediment load is certainly a relevant contribution to the total discharge, with impacts in the floodplain determination. Considering the stream network slope, the simulated ratio is comparable with reports in the literature [e.g. 28]. The sediment load is mainly constrained by the maximum sediment concentration C_{max} and the depth of the flow, suggesting that better information about C_{max} could improve the simulation of flood spots.

1.2 Comments on the results and discussion

- **page 21-22, section 4.1:** On the one hand, the model simulated a flood peak in the upper range of the discharge peak assessment and the simulated flood peak occurred 20 minutes earlier than the observed one. On the other hand, when doing the sensitivity analysis on the surface speed parameter, decreasing the runoff velocity, the simulated flood peak is diminished and occurs later. Why didn't you calibrate better the surface speed, as the model is sensitive?

There are a couple of points to consider. First, as mentioned in the manuscript, some reports suggest the peak flow reached the urban area after 2:10 am, and others around 2:40 am. Second, from the point of view of risk management, and having evidence of likely faster speeds in the channel, we wanted to be conservative, and decided to gravitate towards obtaining a discharge in the high end of the interval. And third, after evaluation, the combination of parameters was the best to reproduce not only the 2015 Salgar flooding event, but also the other peak flow events registered during 2015.

- **Page 22, line 506-511:** I think those results are insights of the paper. They should be discussed in the discussion part to confront them to the literature (if there is) and to highlight them.

We agree with the reviewer. We expanded the discussion as follows:

[...] The overall evidence suggests that precedent capillary moisture in the basin plays an essential role in modulating river discharge. This behavior could be linked to the temporal occurrence and relative importance and timing of stratiform and convective formations previously described. During the extreme event, when the soils were already wet, the convective rainfall fraction dominated the hydrograph formation. While stratiform rainfall plays an important role moistening the entire basin, convective rainfall generates considerable runoff, leading to flash flooding. Several authors have argued about the role of convective rainfall triggering flash floods [9, 18, 31, 7, 30, 25, 29, 13, 3, 15, 5, 27, 10, 23, 2], however, to our knowledge no other study has tracked convective and stratiform water in a modeling setting to explore their relative role leading to flash flooding.

- **Page 25, figure 13:** the specific flood peaks are interesting. The simulated values are below the envelop $Q_{\text{peak}} = 97A^{-0.4}$ that make the simulated flood peak consistent with the literature on flash flood (Gaume et al. 2009). You should mention it on the discussion to strengthen the flood peaks simulation consistency.

We thank the reviewer for pointing this out. We included this comment in the discussion section:

The methodology implies changes and additions to the TETIS distributed hydrological model including tracking independently convective and stratiform precipitation within the model, as well as keeping track of the runoff and subsurface portions of the streamflow. TETIS was coupled with a shallow landslide submodel and HydroFlash, a one-dimensional floodplain scheme. The model proposed here indeed allows studying the different hydrological processes relevant to flash flood and landslide occurrence by using different simulation resources, serving as the basis for a better understanding of the overall basin response. **Despite the lack of data, the evidence suggest that the results represents, to a large degree, the magnitude of the disaster; considering also that the simulated peak flow is consistent with the peak flow envelope proposed by [14] for flash floods.** This approach helps to examine the first-order flood-generating mechanisms or causative factors both in time and in space, focusing on the most important physical processes [20, 24], potentially allowing the anticipation of flash flooding events, the issue of warnings, and response by risk management entities.

- **Page 27, line 595-600:** I think my previous comment was misunderstood. I think you were right saying: “In event 2, the convective rainfall and the runoff show a similar evolution, denoting a strong influence of the convective portion (figure 12b)”. But I think there were one unmentioned condition to observed similar evolution. The similar evolution comes from the fact that the convective portion is totally controlling the runoff processes AND that there is no effect of the stream network to modify or temporize the runoff advent at the outlet. In other words, it’s possible to get strong influence of the convective rainfall runoff without having similar evolution, if the stream network buffers the runoff advent.

We agree with the reviewer. We changed the paragraph to: According to Figure ??b for Event 2, the accumulations of streamflow runoff and convective rainfall become similar with the increase in time. This fact highlights the strong control that, in this case, the convective portion has on the runoff, with almost no effect of the stream network filtering out the convective signal, most likely due to the size and the rapid response of the basin. This description, however, only applies for the runoff portion, since the evolution is different when we consider the total simulated streamflow.

- **Page 27, line 615-617** about the soil depth definition: You justified here the scaling factor by adjusting an underestimated soil depth observation. But then it means that the soil depth definition previously chosen for your hydrological model are also underestimated. I would rather assume that you need to calibrate the model to make the landslide occurring. The scaling factor might explained as to be an artifact of a too simplistic model, and a non calibration of the other parameters.

We partially agree with the reviewer. However, results of the landslide model in other regions show good agreement with observations [1]. In our case we only have a poor and a general description of the watershed soils, that does not allow us to obtain distributed soil maps. This includes soils properties relevant for the model that we did not include. We added a comment about this in the discussion section. See the answer to the last issue raised by the reviewer.

- **Page 29, line 631-632:** This comment should appear in the end of the discussion or in the conclusion, not in the result section.

We agree with the reviewer. We moved the comment to the conclusions section:

Results of the landslide submodel and HydroFlash, while satisfactory, are far from perfect, showing significant differences compared to observations. The evidence suggests, by and large, that most of the observed differences are mainly due to the lack of higher spatial resolution DEM, in the case of HydroFlash, and due to the lack of a detailed soil dataset, in the case of the landslide submodel. However, there is also considerable room for improvement in both submodels, including a better representation of non-Newtonian hydraulic processes in HydroFlash, and a direct link between landslides and flood spots following, for example, a

similar strategy to the one presented in the STEP-TRAMM model [11]. Notwithstanding the difficulties, the results suggest that the submodel simulations could have been used and should be used in the future for early detection and warning to improve both short- and long-term risk reduction strategies.

- **Page 31, line 669-670:** I would refer to Zocatelli et al (2011) as following “Zocatelli et al (2011) found similar results in … (where, and which size of catchement).” As you wrote, it seems that Zocatelli et al (2011) found your own results.

We modified the paragraph following the suggesting by the reviewer:

The evolution of the simulation of Events 1 and 2 show evidence of remarkable behavioral differences. During Event 1, both gravitational and capillary tanks are filled along and across the basin as a result of the quasi-homogeneous rainfall spatial distribution. [36] found similar results for watersheds in Europe with areas ranging between 982 and 52 km². The return flow is low, and most of the runoff occurs within the first 20 groups (40% of the watershed closest to the outlet). In the period between both events, there is a recession in the capillary and gravitational storages in the entire basin. Capillary storage decays considerably slower than gravitational storage. During Event 2, the flash flood triggering event, the first convective core saturates both capillary and gravitational storages in the upper part of the basin and generates both return flow and significant runoff. Due to soil saturation, the second convective core results mainly in surface runoff. During this event, extreme runoff rates are evident in the upper part of the basin, collocated with the steeper slopes. On the other hand, subsurface flow is more important in magnitude than runoff describing Event 1, while runoff is more relevant for Event 2. The precedent storage and the presence of thunderstorm training profoundly condition the streamflow during Event 2. The overall evidence suggests that precedent capillary moisture in the basin plays an essential role in modulating river discharge. This behavior could be linked to the temporal occurrence and relative importance and timing of stratiform and convective formations previously described.

- **Discussion:** As said before, it would be nice if the results of the landslide model and of the floodplain model are discussed. Here some ideas for the landslide model. The facts:

- your model relates landslides to soil depths, soil water content and topography. the soil depth spatial distribution is roughly done according to the topography.
- Landslide occurring is therefore only related to soil filling and the combined ‘topographical-soil depth properties’.
- 1) Crossing topographical map and false simulated landslides location, those latter ones seem to appear where there are slope greater than 2. Is 20 cm soil depth on a 2 slope realistic? Or could it explain the false simulated landslides?
- 2) The observed landslide is observed where the amount but all the intensities of the rainfall are the highest. Could the rainfall intensity have an impact on landslide and explain why the model is failing (as not taking into account).

We agree with the reviewer, and include the next paragraph in the document:

The landslides submodel presents an overall acceptable performance with limitations in certain regions. In particular, there are some false positives in the middle of the basin. These limitations could be associated with the assumptions and approximations inherent to the submodel, including that it only determines unstable cells by slowly filling the soil matrix with water, which, in this case, given the lack of information, depends on the soil depth derived from the topography, and that the model does not consider instability due to intense rainfall events. The lack of detailed soil depth information could explain the false positives landslides. On the other hand, the relation between landslides and high-intensity rainfall must be explored and included in this kind of models. There is also an apparent contradiction regarding the depth of the soils in the basin: While the values

derived from topography appear to work well for the hydrological model, the depth had to be calibrated to obtain a better representation of landslides. There are two possible explanations for the contradiction, (i) that the soils are in fact thicker in the entire basin, but the calibration of the infiltration and percolation rates corrected the hydrological simulations, and (ii) that the landslides submodel is too simplistic, or that no other parameters were calibrated, possibly resulting in over calibration of the soil depth. This is an aspect that needs to be improved further.

The landslide submodel has been used in a nearby watershed with similar characteristics, but with high-quality distributed information [1]. In that case, the model shows a better performance, which highlights the relevance of the quality of the input data. It is also important to consider that, a pinpoint localization of the unstable cells is still considered a hard task, in part due to the small temporal and spatial scale at which landslide processes take place [1, 8, 35].

2 Technical comments

- **Page 5, line 120:** As said before, keep the same name to call the different submodels of your modelling framework: I would suggest to use ‘hydrological model’ and even use it name ‘Tetis’ (Velez et al, 2002), for the first modelling part; ‘landslide submodel’ for the second modelling part and ‘HydroFlash floodplain submodel’ for the third modelling part.

We accept the suggestion by the reviewer; we now refer by **TETIS** to the hydrological model, and we use the word submodel throughout the document to refer to the **landslide submodel** and to the **HydroFlash floodplain submodel**.

- **Page 5, line 122:** choose to totally insert or remove “assumes infinite sediment supply”.

We opted for inserting the comment in the sentence without the brackets.

- **Page 5, line 123:** ‘hydrological’ and not ‘hydrologic’.

We modified the term throughout the entire document.

- **Page 5, line 122-129:** please put the small description in the order it appears in the text: first the hydrological model, second the landslide submodel, third the HydroFlash floodplain submodel.

We have rewritten paragraph as follows:

The methodology followed in this study is based on a modeling framework using the TETIS hydrological model [34?], modified to include a shallow landslide submodel, and a floodplain submodel termed *HydroFlash*. The TETIS model is a cell-distributed conceptual hydrological model that uses storage tanks and the kinematic wave approximation to simulate the most relevant processes in the basin. The landslides submodel is a stability model that classifies cells into unconditionally-stable, unconditionally-unstable, and conditionally stable depending on geomorphology; conditionally stable cells are further classified as stable or unstable based in their variable water content [1]. HydroFlash corresponds to a low-cost 1D model that assumes infinite sediment supply and estimates the cross-sectional filled area at all time steps based on the liquid discharge and the sediment transport. In addition, the TETIS model was modified to include four virtual tracers to separately explore the role of runoff and subsurface flow, as well as the relative importance of convective and stratiform precipitation in flash flood generation. The assessment of the interactions between runoff, subsurface flow, and convective-stratiform rainfall allows a better understanding of the short-term hydrological mechanisms leading to the flash flood event.

- **Page 6, line 149-153:** From my point of view, I would remove those sentences from this section. The aim of the section is to describe the catchment, not to come back on the objectives of the study. If you want to emphasize the challenge to work with scarce physiographical information, you should mention within the introduction for example when speaking to ungauged catchment (end of line 112 for example).

We completely agree with the reviewer. The comment was not in the original versions of the manuscript, and we added it trying to satisfy some comments by the other reviewer, but we did not do it properly. We have removed the mentioned lines and we stress the challenges in different places of the document.

- **Page 6, line 166:** by brackets, I would say () .

We corrected the issue throughout the entire document.

- **Page 8, figure 3:** please add the zoom number on the first top window.

We have modified the figure labels and its caption. The caption is now the following: **Aerial overview of La Liboriana basin (source: Department of Antioquia).** The top-right panel presents the entire basin, showing the location of key regions detailed in the following panels, in zooms 1 to 5. The stream network is also presented, colored by order, from yellow to deep blue corresponding to orders 1 to 5.

- **Page 8, line 195** and somewhere else in the manuscript: unity should not be in italic font.

We made sure to correct all the units in italic to regular font style throughout the document.

- **Page 10, line 241-242:** remove the sentence “the results of the radar [...]” as the same information is done in the sentence line 238-239.

We have removed the sentence, that was indeed redundant.

- **Page 12, title of the section 3.1:** I would suggest to choose “the hydrological model Tetis” as there is only the description of the model in this section (and not the 2 linked submodels). Or do you consider that the framework consists in the the model plus the analysing tools (tracers and catchment cells grouping)?.

We have decided to follow the reviewer suggestion. The title of the subsection is now: **TETIS hydrological model**. In general, we do consider that the framework includes the TETIS model plus the submodels and the analysis tools, but for the methodology section is less confusing to just refer to the model in the title of the subsection.

- **Page 22, line 510:** please remove “On the other hand”.

We have removed it following the suggestion by the reviewer.

- **Page 22, line 517:** ‘According to the model simulations, the peak flow occurred at approximately 2.20am LT’: Why did you say “approximately” ? You have a solely simulation, that should give exactly one flood peak time.

The reviewer is correct. We have one model simulation and one value for the flood peak time. We have deleted the word **approximately** from the sentence.

- **Page 22, line 521:** when describing the figure: To make easier the manuscript reading, you should mention the studied parameters in the same order they appear in the figure: parameter of the top panel, parameter of the center panel, parameter of the bottom panel.

We agree with the comment. We have modified both, the paragraph and the Figure caption as follows:

Figure 10 shows the results of a sensitivity analysis of the hydrological simulation during the second rainfall event, varying the surface speed, infiltration rate, and the subsurface speed

factors. The aim of the sensitivity analysis is to evaluate the robustness of the overall results, considering the fact that the quality and quantity of some of the watershed information is limited. In the sensitivity analysis, we vary the surface speed factor between 0.01 and 20, the infiltration factor between 0.02 and 20, and the subsurface speed factor between 0.1 and 10. The overall sensitivity results show that the main findings described in the previous paragraphs are, in fact, robust to almost all changes in the mentioned parameters, with the surface runoff associated with convective rainfall controlling the magnitude of the peak discharge during the Event 2. The model's highest sensitivity, and hence the largest uncertainty source, appears to be related to the surface speed parameter (Figure 10a), particularly during the peak flow and the early recession. On the other hand, changes in the infiltration rate factor (Figure 10b) and subsurface velocity factor (Figure 10c) are associated with a simulation sensitivity smaller than 7 and 20% of the peak flow, respectively.

Figure caption: **Hydrological simulation sensitivity analysis.** Similarly as in Figure 9, all panels show the simulated streamflow (purple), and the runoff (green) and subsurface flow (dashed purple) separation. From top to bottom, the panels show the simulation sensitivity to changes in the a) surface speed, b) infiltration rate, and c) subsurface speed factors.

- **Page 23, line 534:** please define the acronym 'SIATA'.

The acronym is defined in the **Rainfall information** subsection. SIATA stands for *Sistema de Alerta Temprana de Medellín y el Valle de Aburrá*, which translates to Early Warning System of Medellin and the Aburrá Valley.

- **Page 23, line 545:** write 'skillfully' and 'skillfully'.

We have corrected the typo.

- **Page 24, figure 11:** write 'top', 'center' and 'bottom' panels instead of 'left', 'middle' and 'right' panels.

We modified and corrected the caption of the figure and it now refers to the top, middle and bottom panels.

- **Page 27, line 617 and table 4, page 19:** The scaling parameter for the soil depth is not the same within the text and in the table.

The reviewer is right, there was an error in Table 4. We have changed the scalar parameter value in Table 4 to 3.5.

- **Page 28, line 622-624:** I would remove those two sentences.

We removed the sentences as suggested by the reviewer. We modified the paragraph and some of the material was moved to the discussion section.

- **Page 31, line 656:** "abilities" or "capacities" instead of "capabilities".

We rephrased the sentence to avoid the word "capabilities".

- **Page 32, line 691:** Event 1 and 2 as you already choose the brackets to distinguish between convective (stratiform) events.

The reviewer is correct; we changed the sentence to: **During Events 1 and 2, convective (stratiform) average accumulations are 28 (23) and 17 (14) mm, respectively.**

References

- [1] Edier Aristizábal, Jaime Ignacio Vélez, Hernán Eduardo Martínez, and Michel Jaboyedoff. SHIA_Landslide: a distributed conceptual and physically based model to forecast the temporal

and spatial occurrence of shallow landslides triggered by rainfall in tropical and mountainous basins. *Landslides*, 13(3):497–517, 2016.

[2] H. Baltaci. Meteorological analysis of flash floods in artvin (ne turkey) on 24 august 2015. *Natural Hazards and Earth System Sciences*, 17(7):1221–1230, 2017.

[3] A. Berne and W.F. Krajewski. Radar for hydrology: Unfulfilled promise or unrecognized potential? *Advances in Water Resources*, 51:357 – 366, 2013. 35th Year Anniversary Issue.

[4] Keith Beven. Kinematic subsurface stormflow. *Water Resources Research*, 17(5):1419–1424, 1981.

[5] G. Bruni, R. Reinoso, N. C. Van De Giesen, F. H L R Clemens, and J. A E Ten Veldhuis. On the sensitivity of urban hydrodynamic modelling to rainfall spatial and temporal resolution. *Hydrology and Earth System Sciences*, 19(2):691–709, 2015.

[6] Steven C. Chapra. *Applied Numerical Methods with MATLAB*. McGraw-Hill, 3rd edition, 2012.

[7] Guy Delrieu, John Nicol, Eddy Yates, Pierre-Emmanuel KIRSTETTER, Jean Dominique Creutin, Sandrine Anquetin, Charles Obled, Georges-Marie Saulnier, Véronique Ducrocq, Eric Gaume, Olivier Payrastre, Hervé Andrieu, Pierre-Alain Ayral, Christophe Bouvier, Luc Neppel, Marc Livet, Michel Lang, Jacques Parent du Châtelet, Andrea Walpersdorf, and Wolfram Wobrock. The Catastrophic Flash-Flood Event of 8–9 September 2002 in the Gard Region, France: A First Case Study for the Cévennes–Vivarais Mediterranean Hydrometeorological Observatory. *Journal of Hydrometeorology*, 6(1):34–52, 2005.

[8] Amod S. Dhakal and Roy C. Sidle. Distributed simulations of landslides for different rainfall conditions. *Hydrological Processes*, 18(4):757–776, 2004.

[9] Charles A. Doswell, Harold E. Brooks, and Robert A. Maddox. Flash flood forecasting: An ingredients-based methodology. *Weather and Forecasting*, 11(4):560–581, 1996.

[10] Audrey Douinot, Hélène Roux, Pierre André Garambois, Kévin Larnier, David Labat, and Denis Dartus. Accounting for rainfall systematic spatial variability in flash flood forecasting. *Journal of Hydrology*, 541:359–370, 2016.

[11] Linfeng Fan, Peter Lehmann, Brian McArdell, and Dani Or. Linking rainfall-induced landslides with debris flows runout patterns towards catchment scale hazard assessment. *Geomorphology*, 280:1–15, 2017.

[12] G.R. Foster, L.F. Huggins, and Meyer L.D. A Laboratory Study of Rill Hydraulics: I. Velocity Relationships. *American Society of Agricultural and Biological Engineers*, 3(27):0790–0796, 1984.

[13] M. Fragoso, R. M. Trigo, J. G. Pinto, S. Lopes, a. Lopes, S. Ulbrich, and C. Magro. The 20 February 2010 Madeira flash-floods: Synoptic analysis and extreme rainfall assessment. *Natural Hazards and Earth System Science*, 12(3):715–730, 2012.

[14] Eric Gaume, Valerie Bain, Pietro Bernardara, Olivier Newinger, Mihai Barbuc, Allen Bateman, Lotta Blaškovičová, Günter Blöschl, Marco Borga, Alexandru Dumitrescu, Ioannis Daliakopoulos, Joachim Garcia, Anisoara Irimescu, Silvia Kohnova, Aristeidis Koutoulis, Lorenzo Marchi, Simona Matreată, Vicente Medina, Emanuele Preciso, Daniel Sempere-Torres, Gheorghe Stancale, Jan Szolgay, Ioannis Tsanis, David Velasco, and Alberto Viglione. A compilation of data on European flash floods. *Journal of Hydrology*, 367(1):70–78, 2009.

[15] David Gochis, Russ Schumacher, Katja Friedrich, Nolan Doesken, Matt Kelsch, Juanzhen Sun, Kyoko Ikeda, Daniel Lindsey, Andy Wood, Brenda Dolan, Sergey Matrosov, Andrew Newman, Kelly Mahoney, Steven Rutledge, Richard Johnson, Paul Kucera, Pat Kennedy, Daniel Sempere-Torres, Matthias Steiner, Rita Roberts, Jim Wilson, Wei Yu, V. Chandrasekar, Roy Rasmussen, Amanda Anderson, and Barbara Brown. The great Colorado flood of September 2013. *Bulletin of the American Meteorological Society*, 96(9):1461–1487, 2015.

[16] Leslie Autumn Golden and Gregory S. Springer. Channel geometry, median grain size, and stream power in small mountain streams. *Geomorphology*, 78(1-2):64–76, 2006.

[17] J Graham. *Methods of Stability Analysis. Slope Instability*. John Wiley and sons, 1984.

[18] Ron Kahana, Baruch Ziv, Yehouda Enzel, and Uri Dayan. Synoptic climatology of major floods in the Negev Desert, Israel. *International Journal of Climatology*, 22(7):867–882, 2002.

[19] M. J. Kirkby and R. J. Chorley. Throughflow, Overland Flow and Erosion. *International Association of Scientific Hydrology. Bulletin*, 12(3):5–21, 1967.

[20] V Klemes. *Probability of extreme hydrometeorological events—A different approach, in Extreme Hydrological Events: Precipitation, Floods and Droughts*. IAHS Publ, 1993.

[21] Jumpei Kubota and Murugesu Sivapalan. Towards a Catchment-Scale Model of Subsurface Small-Scale Process-Based Modelling and Runoff Generation Based on Synthesis of Field Studies. *Hydrological Processes*, 9(May 1994):541–554, 1995.

[22] Maddock T Leopold, L.B. The hydraulic geometry of stream channels and some physiographic implications. *Geological survey professional paper*, 1953.

[23] Maria Carmen Llasat, Raul Marcos, Marco Turco, Joan Gilabert, and Montserrat Llasat-Botija. Trends in flash flood events versus convective precipitation in the Mediterranean region: The case of Catalonia. *Journal of Hydrology*, 541(June 2000):24–37, 2016.

[24] R. Merz and G. Blöschl. A process typology of regional floods. *Water Resources Research*, 39(12):1–20, 2003.

[25] M. Milelli, M. C. Llasat, and V. Ducrocq. The cases of june 2000, november 2002 and september 2002 as examples of mediterranean floods. *Natural Hazards and Earth System Sciences*, 6(2):271–284, 2006.

[26] Julien P.Y. Obrien, J.S. Laboratory analysis of mudflow properties. *Journal of Hydrological Engineering*, 8(114):877–887, 1988.

[27] D. Piper, M. Kunz, F. Ehmele, S. Mohr, B. Mühr, A. Kron, and J. Daniell. Exceptional sequence of severe thunderstorms and related flash floods in May and June 2016 in Germany. Part I: Meteorological background. *Natural Hazards and Earth System Sciences Discussions*, pages 1–30, 2016.

[28] Dieter Rickenmann and Anja Koschni. Sediment loads due to fluvial transport and debris flows during the 2005 flood events in Switzerland. 1007(February):993–1007, 2010.

[29] Shahar Rozalis, Efrat Morin, Yoav Yair, and Colin Price. Flash flood prediction using an uncalibrated hydrological model and radar rainfall data in a Mediterranean watershed under changing hydrological conditions. *Journal of Hydrology*, 394(1-2):245–255, 2010.

[30] M. Šálek, L. Brezková, and P. Novák. The use of radar in hydrological modeling in the Czech Republic – case studies of flash floods. *Natural Hazards and Earth System Science*, 6(2):229–236, 2006.

- [31] Russ S Schumacher and Richard H Johnson. Organization and Environmental Properties of Extreme-Rain-Producing Mesoscale Convective Systems. *Monthly Weather Review*, 133(4):961–976, 2005.
- [32] Jean Serra. *Image Analysis and Mathematical Morphology*. Academic Press, Inc., Orlando, FL, USA, 1983.
- [33] T Takahashi. *Debris flow*. Taylor y francis, 2 edition, 1991.
- [34] J.I Vélez. Desarrollo de un modelo hidrológico conceptual y distribuido orientado a la simulación de crecidas. *Tesis doctoral - Universidad Politécnica de Valencia*, page 266, 2001.
- [35] Weimin Wu and Roy C. Sidle. and Number Values Agreed Closely With. *Water Resources*, 31(8):2097–2110, 1995.
- [36] D. Zoccatelli, M. Borga, A. Viglione, G. B. Chirico, and G. Blöschl. Spatial moments of catchment rainfall: Rainfall spatial organisation, basin morphology, and flood response. *Hydrology and Earth System Sciences*, 15(12):3767–3783, 2011.

Reconstructing the Salgar 2015 Salgar Flash Flood Using Radar Retrievals and a Conceptual Modeling Framework in an Ungauged Basin

Nicolás Velásquez ^{1,2}, Carlos D. Hoyos ^{1,2}, Jaime I. Vélez ¹, and Esneider Zapata ²

¹Universidad Nacional de Colombia, Sede Medellín, Facultad de Minas, Departamento de Geociencias y Medio Ambiente

²Sistema de Alerta Temprana de Medellín y el Valle de Aburrá (SIATA), Área Metropolitana del Valle de Aburrá (AMVA)

Correspondence to: Nicolás Velásquez (nvelasq@unal.edu.co)

Abstract. On May 18, 2015, ~~severe rainfall~~ a severe rainfall event triggered a flash flood in the municipality of Salgar, located in the northwestern Colombian Andes. This work aims to reconstruct the main hydrological features of the flash flood to better understand the ~~hydrological~~ processes modulating the ~~event occurrence~~ occurrence of the event. Radar quantitative precipitation estimates

5 (QPEs), satellite ~~data information~~, and post-event field visits are used to reconstruct the Salgar flash flood, in an ungauged basin, addressing the relationship among rainfall spatiotemporal structure, soil moisture, and runoff generation during successive rainfall events by using a conceptual modeling framework including landslide and hydraulic submodels. The ~~hydrologic~~ hydrological model includes virtual tracers to explore the role of runoff and subsurface flow ~~, as well as~~ and the relative
10 importance of convective and stratiform precipitation in flash flood generation. Despite potential shortcomings ~~due to the lack of data~~, the modeling results allow an assessment of the impact of the interactions between runoff, subsurface flow, and convective-stratiform rainfall on the short-term hydrological mechanisms leading to the flash flood event. The overall methodology reproduces the magnitude and timing of the La Liboriana flash flood ~~discharge peak~~ peak discharge considerably well, as well as the areas of landslide occurrence and flood spots, with ~~some~~ limitations
15 due to the spatial resolution of the available digital elevation model's ~~spatial resolution~~. Simulation results indicate that the flash flood and regional landslide features were strongly influenced by the antecedent rainfall, which was associated with a northeasterly stratiform event that recharged the gravitational and capillary storages within the ~~model~~. ~~The simulation shows that the antecedent~~
20 ~~rainfall event moistens mode, moistening~~ the entire basin before the occurrence of the flash flood event ~~, modulating the streamflow and modulating the subsurface-runoff partitioning~~ during the flash

flood event. Evidence suggests that the spatial structure of the rainfall is at least as important as the geomorphological features of the basin in regulating the occurrence of flash flood events.

1 Introduction

25 Flash floods are regarded as one of the most destructive hydrological hazards, resulting in considerable loss of human life and high costs due to infrastructure damage (Roux et al., 2011; Gruntfest and Handmer, 2001). Among all different types of floods, Jonkman (2005) shows that flash floods result in the highest average mortality rate per event (3.62%), almost ten times larger than the mortality rate for river floods. Flash floods are usually described as rapidly rising water level events occurring
30 in steep streams and rivers, associated with short-term, very intense convective precipitation systems or orographically forced rainfall events over highly saturated land surfaces and steep terrains (Šálek et al., 2006; Llasat et al., 2016; Douinot et al., 2016). Convective precipitation episodes often feature high intensity, short duration, and relatively reduced spatial coverage (Houze, 2004).

Several authors have assessed the role of the geological and geomorphological features of the
35 catchment, soil type, soil moisture conditions, and the spatiotemporal structure of rainfall on flash flood occurrence, trying to identify the leading causative mechanisms of this hazard (Merz and Blöschl, 2003). Adamovic et al. (2016) and Vannier et al. (2016) tried to understand the governing processes of flash floods from the geological formation of the basin with mixed results. Wu and Sidle (1995) emphasized the role of the topography, ground cover, and groundwater in the occurrence of
40 shallow landslides and associated debris flows. Due to their rapid nature, flash floods are more likely to occur in small and steep basins (Younis et al., 2008); ~~many~~ Many authors have assessed the influence of hills and stream slopes, suggesting the slopes of the hills are significantly more important for flash flood occurrence and magnitude than the slope of the stream (Šálek et al., 2006; Roux et al., 2011; Yatheendradas et al., 2008). Rodriguez-Blanco et al. (2012) analyzed ~~fifty-four~~ flash
45 flood episodes in Spain and determined that antecedent soil moisture conditions play a vital role in runoff production. Castillo et al. (2003), using a modeling approach, also suggested an important flash flood ~~occurrence~~-dependence on antecedent moisture conditions. Aronica et al. (2012) used spatial and statistical analysis to reconstruct landslides and deposits, finding a connection between flash flood occurrence and soil moisture antecedent conditions.

50 The fact that small basins are more prone to flash floods increases their intrinsic physical and measurement uncertainty (~~Wagener et al., 2007~~, posing difficulty in of the latter (Wagener et al., 2007), making difficult their prediction (Hardy et al., 2016; Ruiz-Villanueva et al., 2013; Yamanaka and Ma, 2017; Borga et al., 2011; Marra et al., 2017) and underlining the need for high spatiotemporal resolution precipitation data (Norbiato et al., 2008). Given the critical role of precipitation, some authors
55 follow a climatological approximation to assess the recurrence of flash floods in particular regions, focusing on the atmospheric causative mechanisms. For example, Kahana et al. (2002) examined

the extent to which floods in the Negev Desert are the outcome of climatological synoptic-scale features, finding that approximately 80% of the events can be linked to distinct synoptic conditions occurring days prior to the flood events. Schumacher and Johnson (2005) studied extreme rain events 60 associated with flash flooding in the United States over a 3-yr period, using the national radar reflectivity composite data to examine the structure and evolution of each extreme rain event. The use of radar data to study flash flood-generating storms is vital for understanding and forecasting these events (National Research Council 1996). Schumacher and Johnson (2005) found that 65% of the total number of ~~episodes~~ flash floods are associated with mesoscale convective systems (MCSs), with 65 two recurrent patterns of organization: the existence of training convective elements and the generation of quasi-stationary areas of convection with stratiform rainfall downstream. Fragoso et al. (2012) analyzed storm characteristics and ~~required~~ rainfall conditions for flash flood occurrence at Madeira (Portugal), and their results suggest an essential role of global climate patterns (North Atlantic Oscillation -NAO- forcing) and local forcing (orographic features) in the triggering of such 70 events. Implicitly, these studies and all the others available in the peer-reviewed literature point to the need for local and regional high-quality spatiotemporal rainfall data. Berne and Krajewski (2013) highlighted the need to incorporate high-resolution weather radar information, even with some limitations, in flash flood hydrology.

The topography of Colombia is characterized by three branches of the Andes crossing the country 75 south-to-north, generating a mixture of landscapes from high snow-capped mountains, vast highland plateaus, ~~and~~ deep canyons to wide valleys, making some regions highly prone to flash flood occurrence. The likelihood of flash flood occurrence in Colombia is also high due to the spatiotemporal behavior of the Intertropical Convergence Zone, and the direction of the near-surface moist air flow leading to orographic enhancement of convective cores (Poveda et al., 2007). In the last decade, 80 there have been several widespread and localized flash flood events in Colombia associated with climatological features and the local intensification of rainfall events. ~~The~~ According to estimates by the "Comisión Económica para América Latina y el Caribe", the 2010-2011 La Niña event alone triggered 1233 flooding events and 778 mass removal processes in Colombia, with more than 3 million people affected and damages estimated ~~by the "Comisión Económica para América Latina y el Caribe"~~ at more than 6.5 billion US dollars. 85

After the 2010-2011 widespread disaster, several isolated events have occurred in the country with devastating consequences. The present paper focuses on studying the processes triggering a flash flood in La Liboriana basin, a 56 km² basin located in the western range of the Colombian Andes, as a result of consecutive rainfall storms that took place between May 15 and May 18, 90 2015. The resulting flash flood dramatically affected the region, causing more than 100 casualties, affecting several buildings and critical infrastructure, and resulting in a total reconstruction cost estimated at 36,000 million Colombian pesos (approximately 12.5 million dollars considering the 2018 exchange rate), which corresponds to three times the annual income of the municipality. Figure



a) Aerial photograph before the event (2012).



b) Aerial photograph taken after the event (2015-05).

Figure 1. Example of infrastructure damage as a result of the La Liboriana flash flood event on May 18, 2015.

a) Aerial photograph taken before the event (2012), during a mission of the Department of Antioquia's Government, and b) satellite image after the event (2015-05). The images show the destruction of most houses in that particular community, a bridge over La Liboriana, and the main road. All of the houses shown in the 2015 image had to be either demolished or structurally repaired. The images also present changes in the delineation of the main channel as well as considerable erosion in the river margins.

1 shows an example of infrastructure damage as a result of the flash flood event and changes in the
 95 basin's main channel after as a result of the flash flood event, showing considerable river margin and bed erosion. Despite the data scarcity, including of discharge measurements, the analysis of the successive rainfall events triggering the Salgar flash flood provides an interesting case of study for assessing the mechanisms that depend on the soil moisture conditions and rainfall distribution.

La Liboriana basin is a typical case of an ungauged basin (Seibert and Beven, 2009; Beven, 2007; Bonell et al., 2006; Yamanaka 100 (Sivapalan et al., 2003; Seibert and Beven, 2009; Beven, 2007; Bonell et al., 2006; Yamanaka and Ma, 2017), with non-existing detailed records of soils or land use, topographic maps or high-resolution digital elevation models (DEMs), and scarce hydro-meteorological data, certainly not available in real

time. According to Blöschl et al. (2012), there are three ~~methods~~ general strategies for using models ~~in these cases under these conditions~~. The first strategy is to obtain the required model parameters 105 from the historical basin behavior and the morphological characteristics of the basin. This strategy often leads to low model performance (Duan et al., 2006). The second approach is to inherit the hydrological ~~model~~ calibration from a ~~gauged neighboring neighboring gauged~~ watershed, which in this case does not exist. The third method is to parameterize the model based on proxy variables, such as hydraulic information obtained during field visits. In the case of the 2015 La Liboriana basin 110 flash flood, there are no previous historical streamflow records ~~or~~, nor records from a neighboring watershed; thus, we followed the third approach. ~~In this work, we~~ We use precipitation information derived from radar, satellite and aerial images, in addition to post-event field visits, to reconstruct the Salgar flash flood event. This study addresses two broad hydrological issues. The first issue consists ~~of~~ in exploring the relationship between rainfall spatiotemporal structure (Llasat et al., 2016; 115 Fragozo et al., 2012), soil moisture and runoff generation (Penna et al., 2011; Tramblay et al., 2012; Garambois et al., 2013) during the successive rainfall events, and the second issue in proposing a simplified ~~hydrologic~~ hydrological modeling scheme, including landslide and hydraulic submodels, to assess the potential occurrence of flash flood events.

The methodology followed in this study ~~includes a hydrological model (Vélez, 2001; ?), is based~~ 120 ~~on a modeling framework using the TETIS hydrological model (Vélez, 2001; Francés et al., 2007)~~, ~~modified to include~~ a shallow landslide ~~model and a flash flood model. The landslide submodel follows the formulation described in (Aristizábal et al., 2016). The hydraulic submodel submodel, and a floodplain submodel termed HydroFlash. The TETIS model is a cell-distributed conceptual~~ hydrological model that uses storage tanks and the kinematic wave approximation to simulate the 125 most relevant processes in the basin. The landslides submodel is a stability model that classifies cells into unconditionally-stable, unconditionally-unstable, and conditionally stable depending on geomorphology; conditionally stable cells are further classified as stable or unstable based in their variable water content Aristizábal et al. (2016). HydroFlash corresponds to a low-cost 1D model (hereafter referred to as HydroFlash) that ~~that~~ assumes infinite sediment supply and estimates the 130 cross-sectional filled area at all time steps. ~~The hydrologic model includes based on the liquid discharge and the sediment transport. In addition, the TETIS model was modified to include four~~ virtual tracers to separately explore the role of runoff and subsurface flow, as well as the relative importance of convective and stratiform precipitation in flash flood generation. The assessment of the interactions between runoff, subsurface flow, and convective-stratiform rainfall allows a better understanding 135 of the short-term hydrological mechanisms leading to the flash flood event. ~~A comparison between the results from both submodels and the observed landslide scars and flooded spots helps to evaluate the overall skill of the proposed methodology.~~

The document is structured as follows. Section 2 describes in more detail the region of study, La Liboriana basin, including geomorphological and climatological characteristics of the basin ~~as well~~

140 as ~~and~~ the information sources used in this ~~study~~assessment. Section 3 presents a description of the overall methodology and the TETIS model used for the reconstruction of the 2015 La Liboriana flash flood event, including flow separation, ~~shallow landslide parameterization, and the proposed model HydroFlash and the shallow landslide and HydroFlash submodels~~. Section 4 describes the main results of the study, including model validation and sensitivity analysis, and presents results
145 from the landslide and HydroFlash submodels. Section 5 includes a discussion on the role of the rainfall structure in the flash flood reconstruction. Finally, the conclusions are presented in section 6.

2 Study site and data

2.1 Catchment description

150 The urban area of ~~Salgar municipality~~ the municipality of Salgar is located near the outlet of La Liboriana basin, a small (56 km²) tropical watershed located in the westernmost range of Colombia's Andes (Figure 2). By 2015, the population of Salgar was estimated at 17,400 persons, 8,800 residing in the urban area. La Liboriana basin joins the El Barroso river basin, and both drain to the Cauca River.

155 The availability of the ALOS-PALSAR DEM (ASF, 2011), with a resolution of approximately 12.7 m, allows estimating the fundamental geomorphological features of the basin. ~~While the resolution of the DEM is far from ideal given the scale of the basin and the main channel, it corresponds to the highest spatial resolution freely available for the region. Additionally, to accomplish the goal of this study, we is to develop and to test a methodology applicable for this type of regions, with scarce information. This is mentioned in a few places in the document, and it has been stressed even more in the current version.~~ The average slope of La Liboriana is 57.6%, and the basin longitude and perimeter are 13.5 km and 57.8 km, respectively. The Strahler-Horton order of the main stream is 5, and its longitude and slope are 18.1 km and 8.1%, respectively. The highest elevation of the watershed (Cerro Plateado) reaches 3,609 meters above sea level (m.a.s.l), while the outlet of the basin is at 1,316 m.a.s.l. The 99th slope percentile of order 1 streams is 78%. For streams of order 160 2, 3, 4, and 5, the 99th slope percentiles are 61, 27, 18 and 11%, respectively. Figure 2 shows the spatial distribution of the slopes in the watershed. These features are typical of Andean mountainous basins. Geomorphologically, this kind of watershed tends to be prone to the occurrence of flash floods (Lehmann and Or, 2012; Penna et al., 2011; Martín-Vide and Llasat, 2018; Longoni et al., 2016; Ozturk et al., 2018; Khosravi et al., 2018; Marchi et al., 2016; Bisht et al., 2018).

170 At the subbasin scale, La Liboriana exhibits a vast range of slopes and altitude differences. Figure 2 shows the height above the nearest drainage ~~"HAND" - (HAND)~~ model (Rennó et al., 2008) for La Liboriana. The ~~"HAND" - HAND~~ calculates the relative height difference between cell *i* and its nearest streamflow cell *j*. La Liboriana ~~"HAND" - HAND~~ exhibits values between 500 and 800 mm. Near the outlet of the basin, over the banks, there are values close to 0 m. High HAND values at the

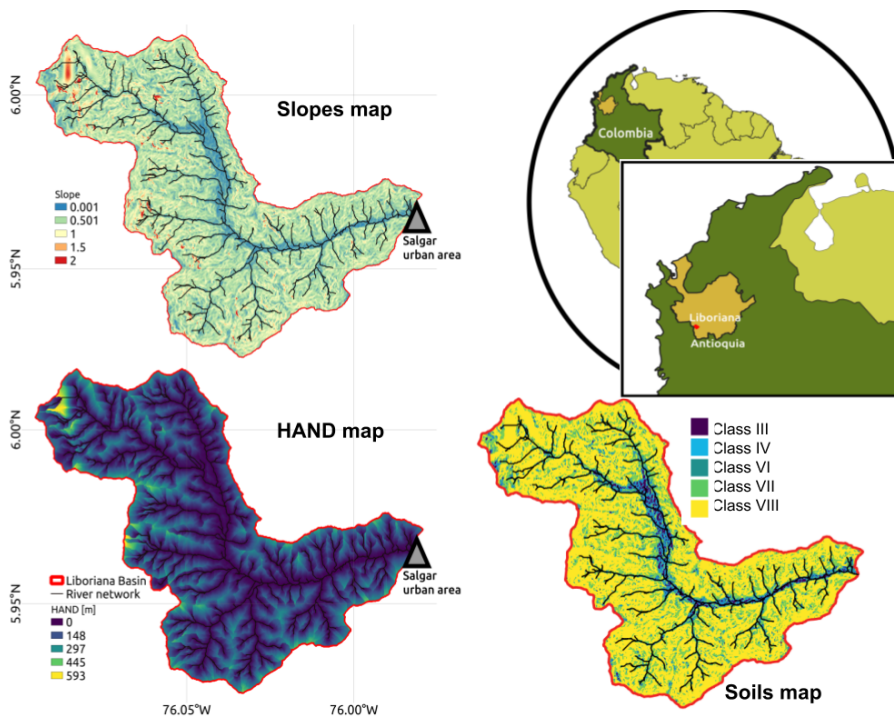


Figure 2. Geographical context of Liboriana basin, located in Colombia, in the Department of Antioquia. The panels include the map of the slopes, the height above the nearest drainage ("HAND"), and the soil type map. The "HAND" values were estimated using ~~the same resolution of the DEM (a 12.7 m-resolution DEM)~~. Low "HAND" values correspond to areas prone to flooding. Note that the soil type map is an extrapolation of the soil properties ~~based on the as a function of~~ slope.

175 upper region of the watershed often denote areas of high potential energy, with increased sediment production and frequent shallow landslide occurrence. Banks with low "HAND" values are more susceptible to flooding and tend to correspond to areas prone to extensive damages caused by extreme events. While the elevation differences described in Figure 2 are typical of the region, the social challenges lie in the high vulnerability of Salgar, given the location of the main urban
 180 settlement.

Vegetation and land use vary considerably within the basin. Figure 3 shows land use in different regions of the watershed from a 2012 aerial image. In the upper La Liboriana basin, there is dense vegetation (see Zoom 1 in Figure 3), with a high percentage of the area covered by tropical forests and ~~the~~ presence of grass and few crop fields. A portion of the upper watershed is considered a
 185 national park. Hillslopes near the divide do not evidence significant anthropic intervention most likely due ~~to the~~ steepness of this region. Down the hills and at the bottom of the valley, there are coffee plantations (the primary economic activity of the region) and pastures. Downstream (Figure 3, Zoom 2), the presence of crops is evident among forest and grass areas. Near the middle of the

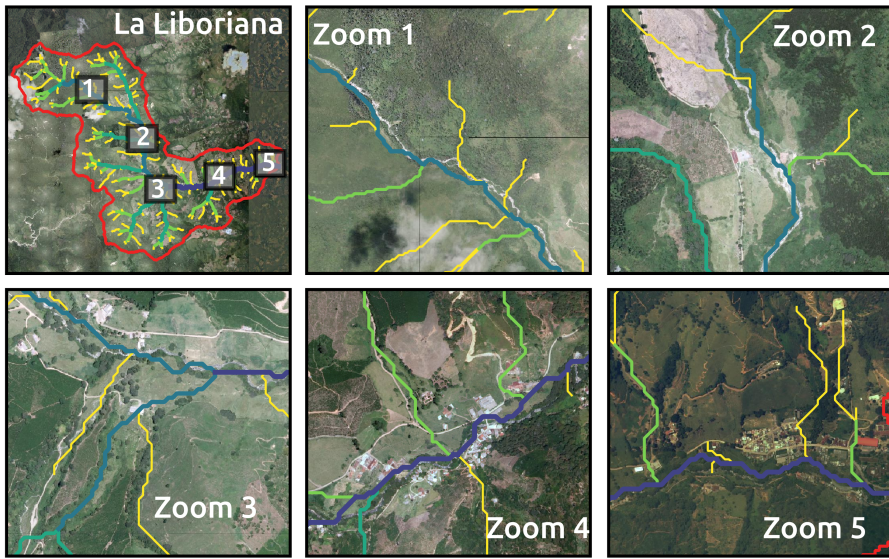


Figure 3. [Land use in different regions](#) [Aerial overview](#) of La Liboriana watershed from a 2012 aerial image basin (Source: Department of Antioquia). The top-right panel presents the entire basin, showing the location of key regions detailed in the following panels, in zooms 1 to 5. The stream network is also presented, colored by order, from yellow to deep blue corresponding to orders 1 to 5.

basin (Figure 3, Zoom 3), the presence of crops is more obvious, and human settlements and roads start to appear. The watershed exhibits grazing areas and urban development near the river banks. In Figure 3, Zoom 4, corresponding to the first affected urban area from upstream to downstream during the flash flood, it is also possible to see a marked presence of crops and some [forest patches](#) [patches of forest](#). Finally, Zoom 5 shows the main urban area of Salgar surrounded by crops, grass and an important loss of forest coverage.

One of the challenges for hydrological modeling and risk management in the country is that soils are not well mapped; the national soil cartography is usually available in a 1:400,000 scale. At this scale, the municipality of Salgar, including La Liboriana basin, corresponds to only one category of soil texture. Osorio (2008), based on field campaign observations and laboratory tests, described La Liboriana soils as [a well-drained soil](#) with poor retention capacity. Organic material is predominant in the first layer, and clay loam soil predominates within the second layer. The depth of the soil is hillslope dependent, varying from 20 [cm](#) to 1 [m](#) (Osorio, 2008). Table 1 provides a summary of soil characteristics for five different categories, all as a function of slope. Each soil category has a corresponding depth and a qualitative description of permeability and retention.

Table 1. Description of the soils in the region (Osorio, 2008).

Type	Slope	Depth [m]	Retention	Permeability	Percentage
Class III	<12	0.6	Low	High	3.2
Class IV	12-25	0.6	Mean	Mean	8.3
Class VI	25-30	1.0	Mean	Mean	2.1
Class VII	30-50	0.3	Too Low	Low	25.5
Class VIII	>50	0.2	Too Low	Low	60.0

2.2 Flash flood post-event observations

205 We conducted a field campaign a few days after the May 18th flash flood ~~event~~ to assess the cross-section geometry along the main channel in different sites, including at the outlet of the basin. During the campaign, we measured sectional distances and the surface water speed ~~at the time of the visit~~, at different points of the streamflow. The surface water speed was measured using a hand-held Stalker Pro II ~~surfacee~~-velocity radar. We also identified traditional post-event terrain, land cover, vegetation
 210 and infrastructure markers to ~~assess the high water marks~~ record the approximate level associated with the peak ~~of~~ flow during the flash flood. Figure 4 presents the selected cross-section used for the estimation of the maximum discharge during the flash flood given its geometrical and hydraulic regularity. The section has a rectangular shape, 4.6 m wide and a height of 5 m for a total area of approximately 23 m². A visual inspection of the flooded house around the section, located 4-5
 215 m away from the channel, reveals the presence of mud marks on the walls with heights varying between 0.5 and 1.2 m (see Figure 4). The area of the section plus the flooded area during the event was estimated to be approximately 37 m². During the campaign, ~~we measured the~~ surface speeds in the channel ~~eseillating varied~~ between 2 and 3 $m s^{-1}$, for a 3 $m^3 s^{-1}$ ~~discharge. In instrumented~~
~~3 s⁻¹ discharge. Instrumented~~ basins in the region, with similar characteristics in terms of area and
 220 slopes, ~~we have recorded~~ show peak flow surface water speeds ~~eseillating ranging~~ between 5 and 7 $m s^{-1}$ (See Figure A.1). By assuming an area of 37 m² and velocities between 5 and 6, we estimate that the ~~observed~~ flash flood peak flow ~~may have been~~ was between 185 and 222 m³s⁻¹. Local authorities reported that the peak streamflow reached the urban perimeter after 2:10 a.m. on May 18th (personal communication during the field visit). ~~Some reports~~ Reports state that the peak
 225 flow in the most affected community occurred at approximately 2:40 a.m¹.

~~There is also relevant aerial~~ Aerial information before and after the occurrence of the event ~~is~~ relevant to analyze the location of the landslides and flooded areas. During 2012, the Department of Antioquia conducted a detailed aerial survey of the ~~Salgar municipality~~ municipality of Salgar, and

¹As reported by the media and the national government: <http://www.elcolombiano.com/antioquia/tragedia-en-antioquia-salgar-un-ano-despues-XX4145514>, https://caracol.com.co/emisora/2015/12/25/medellin/1451076926_792470.html, <http://portal.gestiondelriesgo.gov.co/Paginas/Noticias/2015/Antencion-Emergencia-Salgar-Antioquia.aspx>



Figure 4. Channel cross-section showing an example of flooded infrastructure ~~after~~during the flash flood event. The section shows mud marks on the walls ~~of adjacent houses~~, with heights varying between 0.5 and 1.2 m. ~~These mud stains are evident~~ The houses in ~~buildings~~ the picture are located 4-5 m away from the channel. The photograph also shows the width of the channel and the total estimated depth during the flash flood. The cross-section is ~~located~~ downstream from the bridge shown in the picture.

a few days after the event, DigitalGlobe and CNES/Airbus made available highly detailed satellite images of the same region. We ~~empirically~~ performed a detailed contrast between both products by using a geographic information system (QGIS), which provided us with information about flooded areas and landslide locations (see Figures 1 and 16). Field campaign peak flow estimates and aerial imagery are central to validate the results obtained ~~from the proposed models~~, with the TESTIS model.

235 2.3 Rainfall information

The assessment of the 2015 Salgar flash flood event following a hydrological modeling strategy uses a radar-based QPE technique ~~developed by Sepúlveda and Hoyos (2019)~~ described in Sepúlveda (2016) and Sepúlveda and Hoyos (2017), using radar reflectivity fields using rainfall gauges and disdrometers within the radar domain to obtain spatiotemporal precipitation maps over the basin. ~~A detailed description of the rainfall estimation, as well as the overall meteorological conditions that led to the La Liboriana extreme event, are described in a companion paper (Hoyos et al. (2019))~~. The QPE technique uses retrievals from a C-band polarimetric Doppler weather radar operated by the Sistema de Alerta Temprana de Medellín y el Valle de Aburra (SIATA, a local early warning system from a neighboring region, www.siata.gov.co), located approximately 90 km away from the basin. The radar has an optimal range in a radius of 120 km for rainfall estimation and a maximum operational range of 240 km for weather detection. The radar operating strategy allows obtaining precipitation information every 5 minutes, with a spatial resolution of approximately 128 m. ~~The results of the radar QPE methodology indicate that the rainfall estimation works well within a radius of 120 km~~. Despite the distance between the radar and the basin, and the mountains between

250 them, there are no blind spots for the radar. A comparison between the radar QPE estimates and records from two rain gauges installed three days after the flash flood event show a correlation for an hourly time scale of 0.65. ~~In addition to the rainfall quantification, radar retrievals, before feeding the hydrologic model, are classified in. A detailed description of the rainfall estimation, as well as the overall meteorological conditions that led to the La Liboriana extreme event, are described in~~
255 ~~a companion paper (Hoyos et al., 2019). Radar retrievals are also used to classify precipitation into~~ convective and stratiform areas following a methodology proposed by Yuter and Houze (1997) and Steiner et al. (1995), based on the intensity and sharpness of the reflectivity peaks. The methodology has been widely used in tropical regions as reported in the review by Houze et al. (2015).

260 Between May 15 and May 18, 2015, several storms took place over La Liboriana basin. During the night of May 17, between 02:00 and 09:00 a.m. (local time), a precipitation event covered ~~in~~ almost all of the basin (hereafter referred to as precipitation Event 1). Twenty hours later, between 23:00 p.m. on May 17 and 02:00 a.m. on May 18, two successive extreme convective systems occurred over the basin with the maximum intensity in the upper hills (precipitation Event 2). Event 1 corresponds mainly to a stratiform event ~~that covered almost all of the basin area and incurred with~~
265 an average precipitation accumulation of 47 mm. ~~Event 2 accumulated, on average~~ over the basin, ~~Event 2 corresponds to~~ approximately 38 mm; however, over the upper watershed, the accumulation exceeded 180 mm according to the estimated rainfall amounts based on the radar measurements. Hoyos et al. (2019) show that the individual events ~~duringh during~~ May 2015 were not exceptional, the climatological ~~precipitation~~ anomalies were negative-to-normal, and the synoptic patterns ~~around~~
270 ~~the extreme event associated with the extreme events~~ were similar to the expected ones for the region; ~~however~~, but the combination of high rainfall accumulation in a 96-hour period as a result of successive precipitation events over the basin, followed by a moderate extreme event during May 18, is unique in the available observational radar record, in particular for the upper part of the basin. Figure 5a presents the temporal evolution of the estimated convective-stratiform rainfall partitioning
275 during both Events 1 and 2. The main difference between both events is the timing of the convective versus stratiform participation within each case. Event 1 started as a stratiform precipitation event moving ~~from the southwest~~~~northeastward~~, from the Department of Chocó to the Department of Antioquia across the westernmost Andes mountain range. After 3 hours of stratiform rainfall, training convective cores move over La Liboriana basin generating intense precipitation peaks ~~over in a~~ 2.5
280 ~~hours~~~~hour~~ period. It is important to note that these cores did not strengthen within La Liboriana basin; these systems formed and intensified over the western hills of Farallones de Citará, draining to the Department of Chocó towards the Atrato river. ~~The latter~~ ~~This~~ is not a minor fact because ~~onee~~ ~~the convective system moved with a northeast direction, as a result of the latter process~~, the maximum intensity cores did not fall over the steepest hills of La Liboriana basin but rather near the
285 basin outlet where the slopes are considerably flatter. Figure 5b shows the spatial distribution ~~of~~ cumulative rainfall during Event 1, with the maximum precipitation located toward the bottom third of

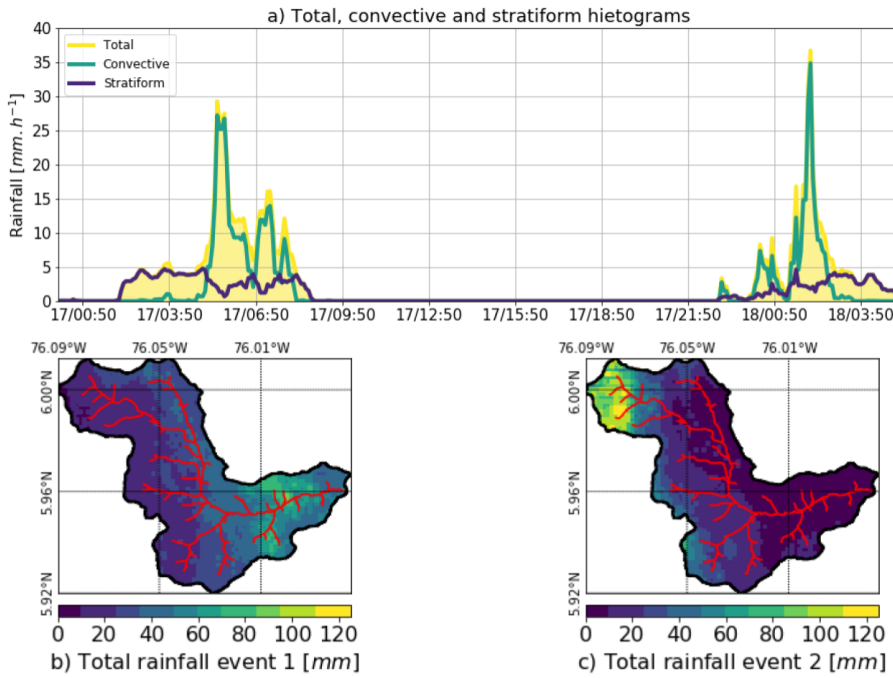


Figure 5. a) Temporal evolution of the convective-stratiform rainfall partitioning during both Events 1 and 2 (units [precipitation intensity](#) in mm per [5-minhour](#), for [5-minute periods](#)). The figure shows the total rainfall (yellow), and the convective (blue) and stratiform (green) portions integrated over La Liboriana basin. b) and c) Spatial distribution of the cumulative rainfall during Events 1 and 2 over La Liboriana basin, respectively.

the basin. Event 2, on the other hand, started as a thunderstorm training event with two convective cores moving from the southeast, followed by the remaining stratiform precipitation. Even though the average cumulative rainfall over the basin was 9 mm less than during Event 1, this event is characterized by orographic intensification within the basin, leading to a more heterogeneous spatial distribution with the highest cumulative precipitation in the steepest portion of the basin (see Figure 5b). [The spatial distribution of Event 2 and highly localized observed intensities most likely led to the flash-flooding episode, as explored in this work.](#)

The data requirements and rainfall preprocessing needed for the overall methodology followed in the reconstruction of the 2015 Salgar flash flood [are summarized in Table 2 and are presented in a schematic diagram in Figure 6.](#)

3 Methodology

3.1 [Hydrological modeling framework](#)[TETIS hydrological model](#)

[The availability of radar-based QPE and a detailed DEM allows the use of a modeling framework based on the distributed hydrologic model. We used a physically-based, distributed hydrological](#)

Item	Description/ Source	Period	Usage
Radar data	QPE rainfall estimations	2015-05-17 to 2015-05-18	Hydrologic model runs. Rainfall TETIS runs, rainfall characterization and event analysis.
Field campaign	Maximum streamflow estimation through visual inspection	2015-05-20	Hydrologic TETIS model comparison for indirect validation.
Satellite imagery	Visible channel compositions from the DigitalGlobe CNES imagery	2015-05 (post-event)	Flash flood model validation, shallow landslides model validation, and comparison with pre-event conditions.
Aerial photos	Aerial photos taken by the government of Antioquia during 2012.	2012	Pre-event conditions comparison.
Soils description	Physical description of the soils of the region by Osorio (2008)	2008	Hydrologic model setup SimulationS using TETIS (model setup).

Table 2. Summary of the data used for the [model setup of TETIS](#).

model developed and fully described in Vélez (2001) and [?with important modifications](#). The hydrologic model simulates different hydrological processes as independent, but with interacting storages (second row, left panel in Figure 6). The model distributes processes by cells with a spatial resolution of 12.7 m (same as the DEM used); in Francés et al. (2007). The spatial distribution and the hydrological flow path schema is based on the 12.75 m-resolution DEM. In each cell, five tanks represent the hydrological processes including capillary (tank 1), gravitational (tank 2), runoff (tank 3), baseflow (tank 4) and channel storage [tanks](#) (tank 5). The state of each tank varies as a function of vertical and lateral flows as shown in [the diagram](#) Figure 6, where the storage is represented by S_i [mm] and the vertical input to each tank by D_i [mm], which in turns depends on the vertical flow through tanks R_i [mm]. E_i [mm] represents the downstream connection between cells, except for tank 1, where E_1 represents the evaporation rate. Vertical flows are only time dependent, while lateral flows could also depend on the actual state of the tank (kinematic approximation).

The model modifications fall in four different categories: (i) the direct use of radar QPE as a source of rainfall information, (ii) the implementation of virtual tracers for surface and subsurface discharge original model is modified to improve the representation of the flow processes that occur during flash floods (see section 3.1.1). In addition, two analysis tools of the TETIS results are introduced: virtual tracers tracking convective and stratiform precipitation as well as [for convective and stratiform water](#)

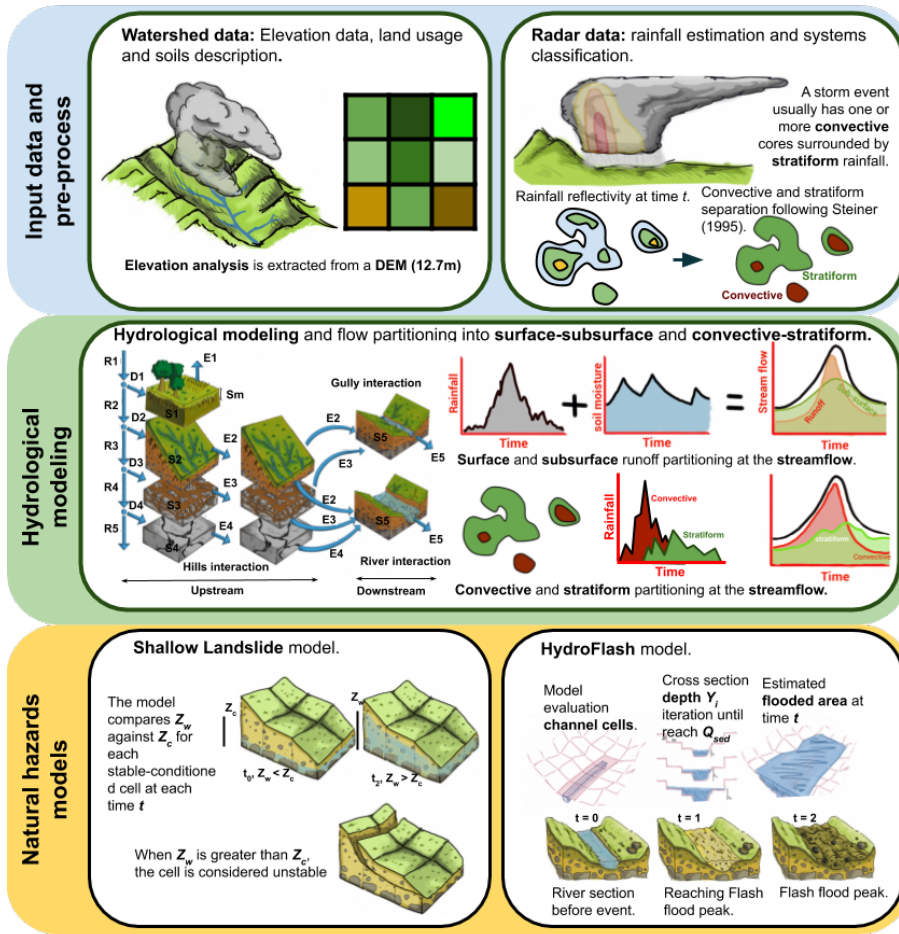


Figure 6. Illustrative diagram of the methodology followed in the present study. The top row represents the availability of key input data, specifically a detailed digital elevation model (DEM) and radar-based QPE as the basis of the modeling framework. The second row represents the mains aspects conceptual basis of the distributed hydrologic TETIS model used. In each cell, five tanks represent the hydrological processes including capillary (tank 1), gravitational (tank 2), runoff (tank 3), baseflow (tank 4) and channel storage tank (tank 5). The state of each tank varies as a function of vertical and lateral flows as shown in the diagram, where the storage is represented by S_i and the vertical input by D_i , which in turns depends on the vertical flow through tanks R_i . E_i represents the downstream connection between cells and evaporation. The implementation of convective and stratiform rainfall separation and virtual tracers is also portrayed. The implementation of the shallow landslides model and HydroFlash submodels are schematized in the bottom row.

tracing, (iii) the enforcement of a maximum gravitational storage (H_g) to allow Hortonian runoff (return flow from S_3 (water paths over or through the soils; and a catchment-state analysis by cell grouping (see Figure 13). The goal is to analyze the spatially distributed response of the watershed to precipitation events of distinct nature.

3.1.1 Lateral flow modeling modifications

The TETIS model relies on the concept of mass balance where the storage of tank 3 to S_2 (tank 2), and (iv) the development of two modules for hazard assessment. The implementation of virtual

325 tracers is represented in the top two right panels of the diagram in Figure 6.i at the end of the simulation interval $S_i(t)^*$ [mm] is function of the storage at the start of the simulation interval $S_i(t)$ [mm] and the storage outflow $E_i(t)$ [mm] during the interval t , as follows:

Additionally, in this study, we propose a graphical method to assess the soil-rainfall-discharge coupling holistically. The first step is to classify all the cells within the watershed in a predetermined 330 number of groups according to their localization and the distance to the outlet. The aim is to establish a coherent and robust spatial discretization, thus allowing the concurrent spatiotemporal variability of the different processes to be summarized in 2D diagrams. Figure ?? shows the watershed grouping

$$S_i(t)^* = S_i(t) - E_i(t) \quad (1)$$

335 The storage outflow E_i is estimated by transforming the storage $S_i(t)$ into an equivalent cross sectional area A_i [m^2], as follows:

$$A_i(t) = S_i(t)F_c/L \quad (2)$$

where L depends on the model cell width Dx [m], Dx for orthogonal flow and $L = \sqrt{2}\Delta x$ for diagonal flow, and F_c [$\text{m}^3 \text{ mm}^{-1}$] is a units conversion factor that is equal to the area of each

340 cell element A_e [m^2] multiplied by 1 m/1000 mm. According to Vélez (2001), E_i changes as a function of localization and distance to the outlet for La Liboriana basin using a 20 and a 50-groups categorization, A_i , the flow speed v_i [ms^{-1}], and the model time step Δt [s], as follows:

Example of watershed grouping as a function of their localization and distance to the outlet for La Liboriana basin using a 20 and a 50-groups categorization.

345 $E_i(t) = A_i(t)^*v_i(t)\Delta t/F_c.$ (3)

3.1.2 Hydrological runoff scheme modification

The expression for the cross sectional area at the end of the simulation period $A_i(t)^*$ is found by replacing $S_i(t)$ in equation (2) for $S_i(t)^*$, and then resulting expression and equation (3) into equation (1),

350 In the model, horizontal flow equations could be either linear or potential, as shown in equation 5

$$A_i(t)^* = \frac{S_i(t)F_c}{L + v_i(t)\Delta t}. \quad (4)$$

Equation (4) is solved coupled with the equation for the speed v_i :

$$v_i(t) = \beta A_i(t)^\alpha \quad (5)$$

Equation 5 is the generic formulation for the speed used in this work to represent nonlinearities in the relationship between v_i and A_i . In the modified hydrologic model formulation, both, β and α are estimated by the user and then implemented in the model change depending on the type of flow: overland, subsurface, base, and channel flow. The solution for v_i is obtained by using the successive substitution method described by Chapra (2012). In the nonlinear approximation, β is a coefficient that summarizes local properties that are invariant over time, such as the slope or the hydraulic conductivity. α is an exponent that changes as a function of the adopted approximation. From equations 5 to 7, $A_i(t)[m^2]$ corresponds to the sectional area of each storage, and $A_i(t)$ varies as a function of the tank storage $S_i(t)[mm]$ according to equation 4. Finally, v_i corresponds to the estimated velocity in m/s model, we use a 5-minute time step which ensures the stability of the computations. When a solution is reached, E_i is computed using equation (3) and S_i is updated using equation (1).

$$v_i(t) = \beta A_i(t)^\alpha$$

Nonlinear equations in lateral flows can result in a better representation of processes at high resolutions (Beven, 1981; Kirkby and Chorley, 1967). A nonlinear approximation of runoff is presented in equation 6. This approximation is a modification of Manning's formula for flow in gullies. According to Foster et al. (1984), ε and e_1 are a coefficient and an exponent used to translate the Manning channel concept into multiple small channels or gullies. The values of ε and e_1 are 0.5 and 0.64, respectively (Foster et al., 1984). $A_{i,2}$ is the corresponding sectional area obtained from $S_{i,2}$ by using equation (4). In addition, $M_{i,0}$ is the slope of the cell, and n_i is the Manning coefficient.

$$v_{i,2} = C_7 \frac{\varepsilon}{n} M_{i,0}^{1/2} A_{i,2}(t)^{(2/3)e_1} \quad (6)$$

The nonlinear equation 7 corresponds to an adaptation of the Kubota and Sivapalan (1995) formula for subsurface runoff, where k_s is the saturated hydraulic conductivity of cell i , and the exponent b is dependent on the soil type, assumed and it is assumed to be equal to 2. A_g is the equivalent cross-section area of the maximum gravitational storage ($H_g[mm]$). A_3 is the equivalent cross-section area of the gravitational storage ($S_3[mm]$) obtained by using equation (4). $A_{i,3}$ is the corresponding sectional area of the gravitational storage ($S_{i,3}$) obtained by using equation (4). There is also return flow from tank 3 to tank 2, when $S_3 = H_g S_{i,3} = H_{i,g}$, which

represents runoff generation by saturation. In the case of the base-flow, we assume that the speed $v_{i,4}$ is constant for each cell and depends on the aquifer hydraulic conductivity $k_{i,p}$ (see equation 8).

$$\underline{v_{i,3}} = C_8 \frac{k_{i,s} M_{i,0}^2}{(b+1) A_{i,g}^b} A_{i,3}(t)^b \quad (7)$$

385

$$\underline{v_{i,4}} = C_9 k_{i,p} \quad (8)$$

Finally, the stream flow velocity is calculated by using the ~~kinematic geomorphological wave~~ (Vélez, 2001; ~~2~~) ~~geomorphological kinematic wave approximation~~ (Vélez, 2001; Francés et al., 2007), in which ~~a [km²] Λ [km²]~~ represents the upstream area, ~~and~~ Ω ~~a~~ and ω_i , a regional coefficient and ~~regional coefficient, and ω_i regional exponents~~ exponents, respectively.

$$\underline{v_{2i,5}} = \frac{\varepsilon}{n} S C_{10} \Omega M_{i,0}^{1/2\omega_1} \Lambda_i^{\omega_2} A_2(t)^{(2/3)\omega_1 \omega_3} \quad (9)$$

$$\underline{v_3} = \frac{K_s S_o^2}{(b+1) A_g^b} A_3(t)^b$$

395 $\underline{v_4} = K_p$

$$\underline{v_5} = \Omega S_{i,0}^{\omega_1} \alpha_i^{\omega_2} A_5^{\omega_3}$$

The equations (6) and (7) describe the momentum of a kinematic wave approximation. In both cases, the velocity depends on the tank storage. These relations are summarized in equation 5 and 400 could be solved numerically when coupled with a mass-balance equation (equation 4). This equation takes into account the storage at each time step ($S_i(t)$), the longitude of the element (Δx), the time step size (Δt), and the speed estimated for the flow in the time step ($v_i(t)$). Equation 4 is related to equation 5 through the velocity term for that tank (v_i) and the cross-sectional area of the tank (A_i). The solution to v_i is obtained by using the successive substitution method (Chapra, 2012) on 405 the mentioned equations. Finally, the total outflow from the tank is calculated using equation 3, in which $E_i(t)$ [mm] represents the outflow from an storage at time step t .

$$\underline{A_i(t)} = \frac{S_i(t)}{\Delta x + v_i(t) \Delta t}$$

$$\underline{E_i(t)} = A_i(t) v_i(t) \Delta t$$

410 On the other hand, equation (8) corresponds to a linear approximation. In this case, the model assumes the speed as a constant value over time, and the total outflow from the tank is estimated

through a linear tank approximation (equation (??)). Under this approximation, $L[m]$ corresponds to the length of the cell, which is Δx when the downstream connection is orthogonal and $\Delta x\sqrt{2}$ when it is diagonal.

415
$$E_i(t) = 1 - \frac{L}{v_i \Delta t + LS_i(t)}$$

The solution for v_i is obtained by using the successive substitution method described by Chapra (2012). In the model we use a 5-minute timestep which ensures the stability of the computations. An extended discussion of the regional parameters can be found in Vélez (2001). The streamflow speed expression is a version of equation (5). This considering that the terms Ω , $M_{i,0}^{\omega_1}$, Λ^{ω_2} , and the exponent ω_3 are constant with time.

3.1.2 Virtual Tools for spatial analysis of the results: virtual tracers and catchment cell grouping

Virtual tracers are implemented in the model to discriminate the streamflow ~~source in superficial sources into surface~~ runoff and subsurface flow, and to assess the portion of streamflow from convective rainfall and stratiform precipitation, recording the source ~~of water~~ at each time step and ~~for~~ each cell. The model archives the results of the virtual tracing algorithm at the outlet of the basin and ~~at for~~ each reach, allowing the study of the role of flows of different ~~natures~~ ~~nature~~ during extreme events at different spatial scales, thereby ~~obtaining more insights about the soil-driven providing insight about the soil-dependent~~ flow regulation.

The flow ~~separation tracing~~ module operates in tanks 2 (runoff storage) and 3 (subsurface storage). 430 The module marks water once it reaches ~~any of those two~~ ~~either of these~~ tanks, and the runoff-subsurface flow percentage is taken into account once the water enters tank 5 (the channel). At this point, the scheme assumes that the water in the channel is well mixed, implying that the flow percentage is constant until ~~a new inflow~~ ~~new water~~ enters the channel.

With a similar concept, the model also follows convective and stratiform rainfall. For this, at each 435 time step, the model takes into account the rainfall classified as convective or stratiform and assumes that at each particular cell, the precipitation is either entirely convective or entirely stratiform. This assumption could lead to estimation errors at basins represented by coarse cells (low DEM resolution) where convective and stratiform precipitation are likely to coexist. In the present study, the spatial resolution of the DEM is 12.7 m, higher than the resolution of the radar retrievals (approximately 125 m), so the potential convective and stratiform rainfall concurrence is very low, and it could not be identified using the Steiner et al. (1995) approach.

~~Additionally, we propose a graphical method to analyze, at the same time, the evolution of multiple hydrological variables in the entire basin. The first step is to classify all the cells within the watershed in a predetermined number of groups according to their localization and the distance to the outlet.~~

445 The aim is to establish a coherent and robust spatial discretization, thus allowing the concurrent spatiotemporal variability of the different processes to be summarized in 2D diagrams.

3.1.3 ~~Hydrologic~~ **TETIS** model calibration

The ~~hydrologic~~ **TETIS** model requires a total of 10 parameters. Table ?? includes all the parameters used in the model. The values of the parameters were derived from the soil properties described in 450 section 2. Due to the lack of detailed information in the region, parameters such as the infiltration and percolation rates are assumed to be constant in ~~all of the~~ ~~the entire~~ basin. Other parameters, such as the capillary and gravitational ~~storage~~ **storages**, vary as a function of the geomorphological characteristics of the basin such as the elevation and slope. The calibration consists of ~~scaling~~ **finding** ~~the optimal scaling for~~ each physical parameter ~~by~~, **using** a constant value ~~in~~ **for** the entire basin (??) 455 (Francés et al., 2007). The model simulation is set to reach a base flow of $3 \text{ m}^{3\text{s}^{-1}} \text{s}^{-1}$, a value that corresponds to the discharge measurements during field campaigns days and weeks after the flash flood event ~~and~~, during dry spells. To set the soil wetness initial conditions realistically, the model **runs** **simulations** start two days prior to Event 1. Before this period, there were only a couple of ~~small~~ ~~weak~~ rainfall events; for this reason, the overall wetness was set to represent **to** dry conditions at the 460 start of the simulation. Table ?? ~~includes~~ **shows** the mean value for all of the parameters used in the model, and the scalar ~~value is~~ **factor** adjusted during the model calibration. ~~In this implementation of the model, we left uncalibrated the channel speed, the subsurface speed, the aquifer losses, and the capillary and gravitational storages phase. For the 2015 Salgar flash flood reconstruction, we calibrate the evaporation rate, the infiltration, the percolation, the overland flow speed, and the~~ 465 ~~subterranean flow speed~~ (see Table ??). The values for ~~these~~ **not calibrated** parameters are inherited from a local watershed with similar characteristics.

3.2 ~~Shallow landslide~~ **Landslide** submodel

The ~~shallow~~ landslide submodel coupled to the ~~hydrologic~~ **TETIS** model is proposed by Aristizábal et al. (2016). The stability of each cell is calculated through the assessment of the different stresses applied to the soil. ~~The matrix. The coupling between TETIS and the landslide submodel is required because the~~ stability of the soil decreases with the pore water pressure (Graham, 1984). The ~~slope failure occurs when the saturated soil thickness above the slip surface~~ ~~saturated soil depth~~ $Z_{i,w}$ (~~equation (10)~~), which depends on the gravitational storage $S_{3,i}(t)S_{i,3}(t)$, the soil wilting point $W_{i,pwp}$, and the soil field capacity $W_{i,fc}$, **as follows**:

$$475 Z_{i,w}(t) = \frac{S_{i,3}(t)}{W_{i,fc} - W_{i,pmp}} \quad (10)$$

When $Z_{i,w}$ is greater than a critical saturated the critical depth $Z_{i,c}$ (equation (11)), failure occurs.

The critical saturated depth depends on the shallow soil depth Z_i , the soil bulk density γ_i , the water density γ_w , the gradient of the slope $\beta_{i,0}$, the soil stability angle ϕ_i , and the soil cohesion C'_i .

$$Z_{i,c} = \frac{\gamma_i}{\gamma_w} Z_i \left(1 - \frac{\tan \beta_{i,0}}{\tan \phi_i} \right) + \frac{C'_i}{\gamma_w \cos^2 \beta_{i,0} \tan \phi_i} \quad (11)$$

480 Figure 7 describes the variables of the model and the balance of forces considered, and Table 3 presents the required parameters for this model.

$$Z_{i,w}(t) = \frac{S_{3,i}(t)}{W_{i,cfc} - W_{i,pmp}}$$

$$Z_{i,c} = \frac{\gamma}{\gamma_w} Z_i \left(1 - \frac{\tan \beta_i}{\tan \phi_i} \right) + \frac{C'}{\gamma_w \cos^2 \beta_{i,0} \tan \phi_i}$$

485 According to the soil stability definition, the topography and the soil properties, all cells are classified into three classes: unconditionally stable, conditionally stable and unconditionally unstable. In particular, three parameters determine the stability of each cell: (i) residual soil thickness-water table $Z_{i,min}$ (equation (12)), (ii) the maximum soil depth at which a particular soil remains stable $Z_{i,max}$ (equation (13)), and (iii) the maximum slope at which the soil remains stable $\beta_{i,0}$ (equation (14)).

$$Z_{i,min} = \frac{C'_i}{\gamma_w \cos^2 \beta_{i,0} \tan \phi_i + \gamma_i \cos^2 \beta_{i,0} (\tan \beta_{i,0} - \tan \phi_i)} \frac{C'_i}{\gamma_w \cos^2 \beta_{i,0} \tan \phi_i + \gamma_i \cos^2 \beta_{i,c} (\tan \beta_{i,0} - \tan \phi_i)} \quad (12)$$

$$Z_{i,max} = \frac{C'}{\gamma_i \cos^2 \beta_{i,0} (\tan \beta_{i,0} - \tan \phi_i)} \frac{C'_i}{\gamma_i \cos^2 \beta_{i,0} (\tan \beta_{i,c} - \tan \phi_i)} \quad (13)$$

495 $\beta_{i,0} = \tan^{-1} \left[\frac{\tan \phi_i}{\gamma_w / \gamma_i} \left(1 - \frac{\gamma_w}{\gamma_i} \right) \right]$ (14)

A cell is unconditionally stable when Z_i is smaller than $Z_{i,min}$ or when the cell slope is smaller than $\beta_{i,0}$. On the other hand, a cell is unconditionally unstable when Z_i is greater than $Z_{i,max}$, and finally, a cell is conditionally stable when Z_i is between $Z_{i,min}$ and $Z_{i,max}$. Shallow landslides are calculated at each time step of the hydrological simulation, based on the latter cell class, where the soil stability depends on the storm event, becoming unstable when $Z_{i,w}(t)$ is greater than $Z_{i,c}$.

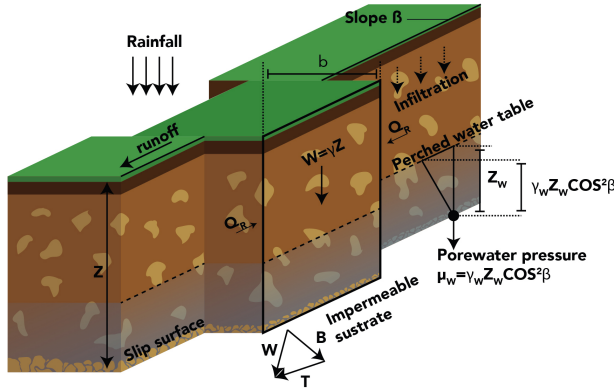


Figure 7. Schematic diagram of the [geotechnical-conceptual model](#) [landslide submodel](#). The figure and description are adapted from Aristizábal et al. (2016). Q_L and Q_R are the resultant forces on the sides of the slice [of soil](#).

Parameter Name	Symbol	Scalar Parameter	Mean Value	Spatial distribution
Soil depth	Z_i [mm]	0.3 3.5	300	As a function of the slope
Topography slope	$\beta_{i,0}$ [adim]	1	0.01 - 5.3	From the DEM
Soil bulk density	γ_i γ_{ed} [KNm^{-3} KNm⁻³]	1	18	Assumed constant
Water density	γ_w [KNm⁻³ KNm⁻³]	1	9.8	Constant
Soil stability angle	ϕ_i [0]	1	30 0	Assumed constant
Soil cohesion	C'_i [KN]	1	4	Assumed constant

Table 3. [Shallow landslides](#) [Landslide](#) model parameters.

3.3 Floodplain submodel (HydroFlash)

In this section, we describe the HydroFlash flash model for flash floods. The model extracts the cross-profile from the DEM for each cell considered part of the network, and it estimates flood spots

505 at each network cell during execution time.

The model requires hydraulic parameters for all network cells to determine flash flooding spots. The channel width is estimated using the Leopold (1953) approach $W_i = 3.26 Q_i^{-0.469}$. The channel slope ($S_{i,0}$) is obtained as the mean value of the slopes that correspond to the cells of a hydrological reach. The characteristic diameter $D_{i,50}$ is assumed equal to 0.138 m and constant (Golden and Springer, 2006). 510 The cross-section ($F_{sec,i}$) is obtained from the DEM for every network cell, perpendicular to the flow direction of the cell, $D8_i$, (see step 1 in Figure 8).

For each time step t and for each stream cell, equation 16

The HydroFlash submodel is designed to interpret the TETIS simulations as floodplain inundations (Figure 8). For each stream cell and at each time step, the submodel (i) calculates the stream discharge including sediment load (equations 15 - 20, see Takahashi (1991)), and (ii) determines the height of the water table $Y_i(t)$ using the simulated streamflow $Q_{i,sim}(t)$ and flow velocity $v_{i,sim}(t)$ (step 2 in Figure 8). The model calculates inundated cells according to the stream cross-profile, the sectional area, and the stream velocities when including the sediment load (equations 19 - 21, Takahashi (1991)). To determine the discharge including sediment load ($Q_{i,load}$), a realistic channel width is calculated according to Leopold (1953) approach as

$$W_i = 3.26Q_i^{-0.469} \quad (15)$$

where Q_i corresponds to the streamflow estimated based on a long-term water balance.

Assuming an infinite sediment and rubble supply, equations 16, 17, 18 are used to deduce, from the channel width W_i , the water level Y_i (equation (16)), the friction velocity $v_{i,fr}$ (equation ($v_{fr,i}(t)$)) 515 using $Y_i(t)$ as in equation (17) derived from Keulegan and Rouse equations (Takahashi, 1991; Savage and Sayed, 1984). Equations 18 and 19 allow the estimation of the concentration ($c_i(t)$)¹⁶, described in Takahashi (1991), the sediment concentration c_i (equation (18)), and finally the sediment-loaded stream discharge (equation (20)), as follows:

$$Y_i(t) = \frac{Q_{i,sim}(t)}{v_{i,sim}(t)W_i} \quad (16)$$

530

$$v_{i,fr}(t) = \frac{v_{i,sim}(t)}{5.75 \log \left(\frac{Y_i(t)}{D_{i,50}} \right) + 6.25} \quad (17)$$

$$c_i(t) = C_{max} (0.06Y_i(t))^{\frac{0.2}{v_{i,fr}(t)}} \quad (18)$$

535

$$r_i(t) = \frac{1}{D_{i,50}} \left[\frac{g}{0.0128} \left(c_i + (1 - c_i) \frac{\gamma_w}{\gamma_{sed}} \right) \right]^{1/2} \cdot \left[\left(\frac{C_{max}}{c_i} \right)^{1/3} - 1 \right] \quad (19)$$

$$Q_{i,load}(t) = \frac{Q_{i,sim}(t)}{1 - c_i(t)} \quad (20)$$

where $v_{i,sim}$ and constitutive coefficients ($r_i(t)$), respectively. The constitutive coefficient summarizes the $Q_{i,sim}$ are the simulated velocity and streamflow, respectively. Also, r_i is the constitutive coefficient

540 of the flow, that summarizes the flow dynamics associated with flows containing colliding particles, such as a flash flood (Takahashi, 1991). In general, the characteristics of an apparent fluid are determined by the relationship between the operating shear stress and the rate of strain, known as the constitutive law. In equation 18, C_{max} represents the maximum sediment concentration; according to Obrien (1988) sediments and colliding particles. The above mentioned relationships depend of 2 parameters: the maximum sediment concentration (C_{max} is near [-]) and the characteristic diameter of the sediments $D_{i,50}$ [m]. Both terms are assumed to be constant and equal to 0.75 during flash floods. The streamflow plus estimated sediments and rubble are estimated according to equation 20 (Obrien, 1988) and 0.138 (Golden and Springer, 2006), respectively.

$$545 Y_i(t) = \frac{Q_{i,sim}(t)}{v_{i,sim}(t)w_i}$$

$$550 v_{fr,i}(t) = \frac{v_{i,sim}(t)}{5.75 \log \left(\frac{Y_i(t)}{D_{i,50}} \right) + 6.25}$$

$$c_i(t) = C_{max} (0.06 Y_i(t))^{\frac{0.2}{v_{fr,i}(t)}}$$

$$555 r_i(t) = \frac{1}{D_{i,50}} \left[\frac{g}{0.0128} \left(c_i + (1 - c_i) \frac{\gamma_w}{\gamma_{sed}} \right) \right]^{1/2} \cdot \left[\left(\frac{C_{max}}{c_i} \right)^{1/3} - 1 \right]$$

$$Q_{i,sed}(t) = \frac{Q_{i,sim}(t)}{1 - c_i(t)}$$

Assuming an infinite sediment and rubble supply, $Q_{i,sed}(t)$ corresponds to the maximum streamflow for each section. The flood depth $F_{d,i}(t)$ is computed following equation (22), iteratively, such 560 that the difference between the estimated stream flow ($\hat{Q}_{i,sed}(t)$) (equation 21) To determine the inundated cells, the flood depth ($F_{i,d}$) and the simulated streamflow $Q_{i,sed}(t)$ is less than a predetermined admissible error σ (step 2 in Figure 8). In the process sectional area of the stream including sediments ($A_{i,load}$) are iteratively calculated by reducing the difference between $Q_{i,load}$ and $\hat{Q}_{i,load}$. The channel cross-section for cell i , $E_{i,bed}$, is defined by the DEM. In each iteration N , the model obtains the flooded area $A_{i,sed}$ (equation (23)), the flooded cells for each section $F_{f,i}$ and the flood depth 565 (step 3 in Figure 8) updates $F_{i,d}$ with a $\Delta y = 0.1$ m increase. The cross sectional area $A_{i,load}$ is calculated by taking difference between $F_{i,d}$ and the elevation of each cell j in the cross-section $E_{i,bed}$.

$$F_{d,i,j} \hat{Q}_{i,load}(t) = b0.2 r_i(t) (N \Delta y)^{\frac{3}{2}} S_{i,0} A_{i,load}(t) \quad (21)$$

$$570 F_{d,i}^N = F_{d,i}^{N-1} + \Delta y \quad (22)$$

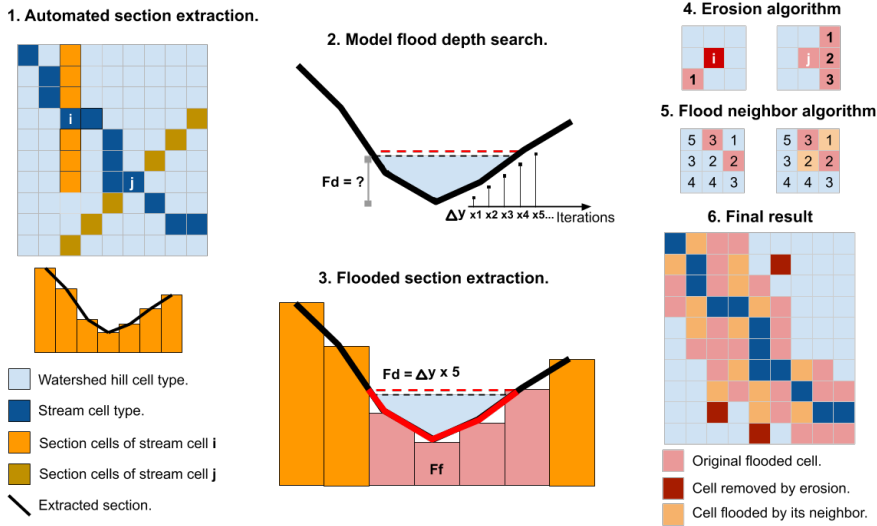


Figure 8. Illustrative diagram of the HydroFlash submodel scheme. **Step 1.** The [model-wmf submodel](#) extracts the cross-profile from the network [considering the DEM and flow direction](#). **Step 2.** [With-Based on](#) equation (21), the [model submodel](#) obtains [at](#) the first approximation [to](#) of the flash flood streamflow; then, the flood depth and [the cross-section](#) area are obtained [with](#) [from](#) equations (22) to (21). **Step 3.** The [model submodel](#) obtains the flooded portion of the cross section. **Step 4.** Erosion post-process. **Step 5.** Filling post-process. **6.** The final result [is acquired](#) for a time step t .

$$A_{i,load}^N = \Delta x \sum_{j=1}^N F_{d,i,j,d} - E_{i,j,bed} \text{ with } E_{i,j,bed} < F_{sec,i,j,d} \quad (23)$$

The resulting flood maps might include the presence of small isolated flood spots and discontinuities where the flow direction changes from orthogonal to diagonal [across](#) or vice versa. We included two post-processing steps to correct these issues by (i) using an image processing erosion algorithm 575 (Serra, 1983) to remove the small [and](#) isolated flood spots (step 4 in Figure 8); [the image erosion is performed once with a 3-by-3 kernel](#). To [and](#), to solve the flow direction discontinuities, (ii) [for](#) each flooded cell [the model](#) seeks to inundate [its](#) [the](#) eight neighboring cells. A neighbor cell is also flooded if the altitude of the original flooded cell, plus the flood depth, is higher than its elevation (step 5 in Figure 8). [The image erosion is performed once with a 3 by 3 kernel](#). An example of the 580 final result for a time step t is shown in the step 6 in Figure 8.

4 Results

The [primary main](#) results of the present study include the reconstruction of the 2015 Salgar flash flood, the assessment of the importance of soil moisture in the [hydrologic-hydrological](#) response of the basin, and the evaluation of the relative role of stratiform and convective precipitation cores in

585 the generation of the observed extreme event. This section is based on the ~~results from the~~ analysis of the hydrological simulation, as well as ~~occurrences the occurrence~~ of shallow landslides and flash floods~~and simulation, and their simulation. A comparison of the results from both submodels and the observed landslide scars and flooded spots allows to evaluate the overall skill of the proposed methodology.~~

590 **4.1 Hydrologic model TETIS validation and sensitivity analysis**

Figure 9a presents the results of the hydrological simulation at the outlet of the basin. The simulation shows that Event 1 generates a hydrograph with a peak flow of $Q_{max} = 160 \text{ m}^3 \text{s}^{-1}$. It is important to note that during ~~precipitation in~~ Event 1, there were no damage or flooding reports by local authorities. Even though this precipitation event did not generate flooding, it set wet conditions 595 in the entire basin before the occurrence of Event 2 (see the purple line in Figure 9b ~~representing the capillary storage~~). Additionally, it is clear from the simulation that during the flash flood event, the two successive convective cores over the same region (training convection) generated a peak flow of $Q_{max} = 220 \text{ m}^3 \text{s}^{-1}$, a value that is in the upper range of the estimated streamflow based on post-event field evidence ($185-222 \text{ m}^3 \text{s}^{-1}$). Figure 9a also presents the simulated runoff and 600 subsurface flow separation as well as the convective-stratiform-generated discharge discrimination. The modeling evidence during Event 2 suggests the convective rainfall fraction dominates the hydrograph formation. In both events, convective (stratiform) precipitation appears to be closely related to the simulated runoff (subsurface flow). ~~On the other hand, the~~ ~~The~~ simulated subsurface flow is more important in magnitude than that runoff in describing Event 1, while runoff is more relevant 605 for Event 2. Figure 9b presents ~~not only~~ the capillary storage (purple), ~~as well as~~ ~~but also~~ the runoff (continuous blue) and the gravitational ~~storage~~ (dashed blue) ~~storage temporal variability~~ ~~temporal variability~~, as represented by the proposed model. As expected, runoff storage is only nonzero during the storm duration, while gravitational storage increases considerably during rain events, followed by a slow recession. There is an increase in basin-wide capillary storage during Event 1, remaining 610 considerably high during the time leading to the occurrence of Event 2. According to the model simulations, the peak flow occurred at ~~approximately~~ 2:20 a.m. LT on May 18th, which is ~~very~~ accurate compared to the reports from local authorities (~~between 2:10 and 2:40 a.m. LT~~), considering all the data limitations.

Figure 10 shows the results of a sensitivity analysis of the hydrological simulation during the second rainfall event, varying the ~~surface speed~~, infiltration rate, and the ~~surface and subsurface speed parameters~~ ~~subsurface speed factors~~. The aim of the sensitivity analysis is to evaluate the robustness of the overall results, considering the fact that the quality and quantity of some of the watershed information is limited. In the sensitivity analysis, we vary the ~~infiltration parameter between 0.02~~ ~~surface speed factor between 0.01~~ and 20, the ~~surface speed parameter between 0.01~~ ~~infiltration factor between 0.02~~ and 20, and the subsurface speed ~~parameter~~ ~~factor~~ between 0.1 and 10. The 620

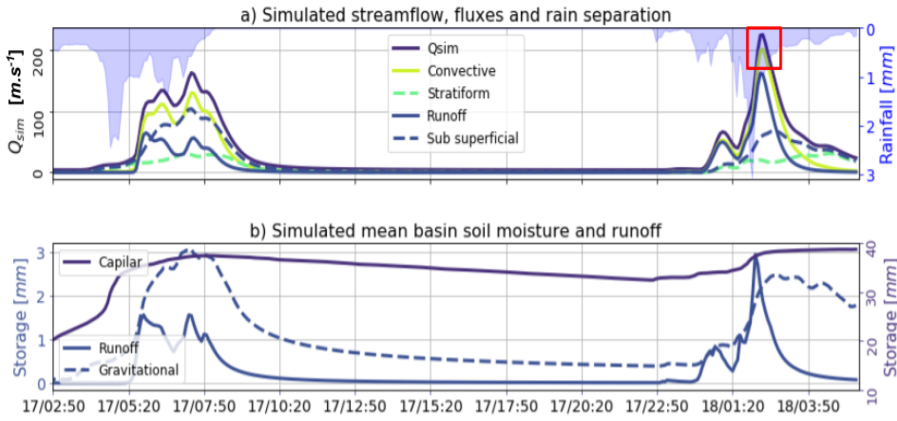


Figure 9. Summary of the results from the [TETIS](#) hydrological simulation. a) Simulated streamflow, [convective-stratiform-generated discharge discrimination, and](#) runoff and subsurface flow separation [and convection-stratiform-generated discharge discrimination](#). The red square represents the flash flood peakflow interval that is estimated based on field campaign evidence. b) [The mean runoff, gravitational Basin average capillary, runoff and capillary gravitational](#) storages during the simulation period.

overall [simulation](#) sensitivity results show that the main findings described in the previous paragraphs are, in fact, robust to almost all changes in the mentioned parameters, with the surface runoff [that is](#) associated with convective rainfall controlling the magnitude of the peak discharge during the Event 2. [Changes in the infiltration rate \(Figure 10a\) result in peak flow changes with a magnitude less than 7%, and changes in the subsurface velocity parameter \(Figure 10e\) lead to peak flow changes with a magnitude less than 20% in the original simulation.](#) The model's highest sensitivity, and hence the largest uncertainty source, appears to be related to the surface speed parameter (Figure 10ba), particularly during the peak flow and [the](#) early recession. [On the other hand, changes in the infiltration rate factor \(Figure 10b\) and subsurface velocity factor \(Figure 10c\) are associated with with a simulation sensitivity smaller than 7 and 20% of the peak flow, respectively.](#)

After the flash flood event, [SIATA installed](#) a stream gauge level station [was installed](#) near the outlet of the basin (see Figure 2). We use these records to validate the model results without further calibration. Since the observed series correspond to [level values](#) [stage level records](#), the streamflow estimation is performed following two different approaches. The first approach, the empirical one, consists of subtracting the 10th percentile of the observed stage time series from the observational record, and the 10th percentile of the simulated streamflow, from the same series. On the other hand, the second method uses the Manning formula. For this, we consider the geometry of the section in Figure 4, and the slope from the DEM. Additionally, due to the potential uncertainties, we consider three different Manning values (0.015, 0.02, 0.03). Figure 11 shows the estimated streamflow using the two methods for four different hydrographs during July, August (2 events) and December 2015. The simulated magnitudes appear relatively close to the observations, and the peak discharge time

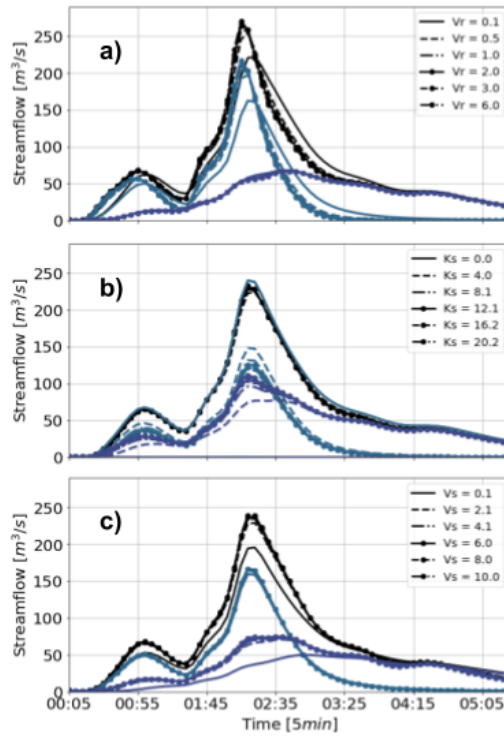


Figure 10. Hydrological simulation sensitivity analysis. Similarly as in Figure 9, all panels show the simulated streamflow (purple), and the runoff and subsurface flow separation. Total streamflow is purple, runoff is (green) and subsurface flow (dashed purple) separation. The left panel shows sensitivity to changes in the infiltration rate parameter, the middle panel shows the simulation sensitivity to changes in the a) surface speed, b) infiltration rate, and the right panel to changes in c) subsurface speed factors.

is captured skillfully in three of the four cases presented. The discharge values using the "high" Manning number estimation (0.015) are similar to the empirical method. The performance of the model is acceptable (Figure 11), considering the lack of calibration, the size of the basin, 645 and the magnitude of the recorded events. The results shown include cases where the peak flow was over-estimated (panels c and d), and under-estimated (panel b).

Figure 12 shows the temporal evolution of discharge during Event 2 in different locations along the watershed's main channel. The upper location corresponds to 15% of the area of the basin, and the other downstream locations correspond to 52%, 76%, and 100% of the watershed. The difference 650 in the time of the peak discharge between the upper location and the outlet of the basin is approximately 35 minutes, which is plausible with travel speeds between 5 and 7 ms^{-1} and an effective distance of 14 km. In terms of volume, approximately 737,000 m^3 of the total 1,438,000 m^3 simulated at the outlet of the basin are generated on the 15% upstream part of the watershed, corresponding to about half of the total mass. In terms of peak flow, due to the slope and velocity 655 changes, the simulated discharge at the 15% upstream part of the watershed corresponds to 50% of

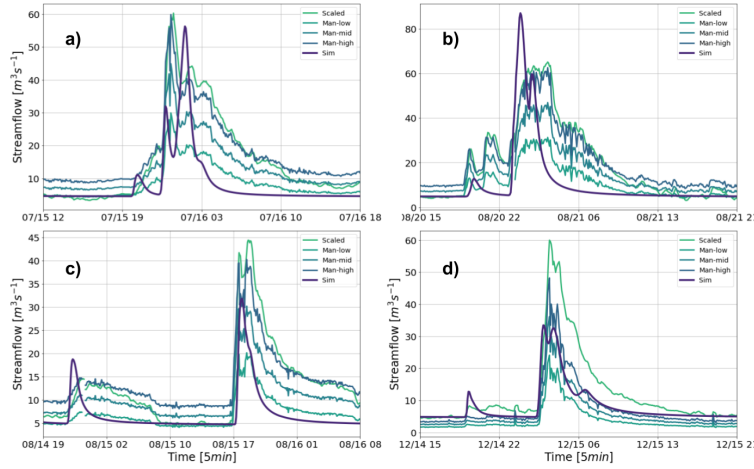


Figure 11. Comparison between hydrological model TETIS simulations and streamflow estimations. The events were observed by from a stage level station installed by SIATA days after Event 2 on a bridge at the outlet of the basin (see Figure 2)

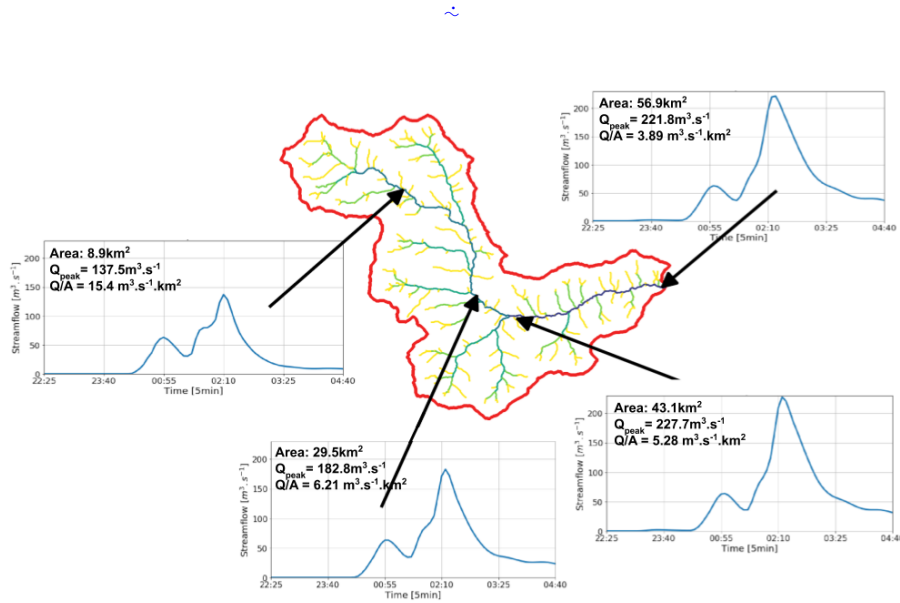


Figure 12. Temporal evolution of discharge during Event 2 in different locations along the watershed's main channel. The upper location corresponds to 15% of the area of the basin, and the other downstream locations correspond to 52%, 76%, and 100% of the watershed, respectively.

the peak discharge at the outlet of the basin.

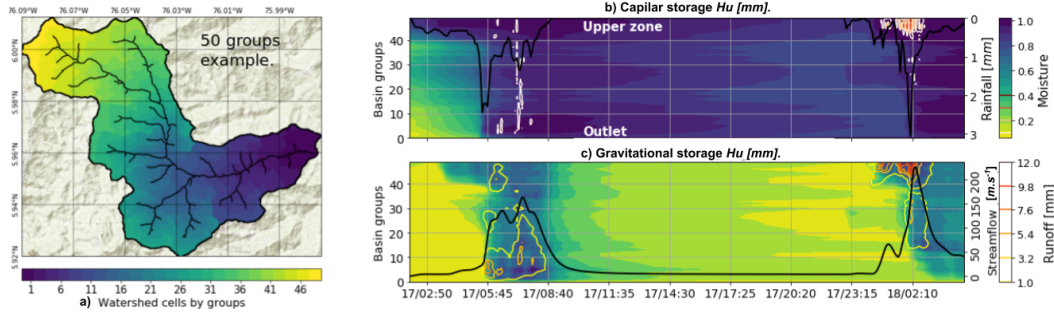


Figure 13. a) Example of watershed grouping as a function of their localization and distance to the outlet for La Liboriana basin using a 50-group categorization. b) Simulated capillary moisture (filled green-to-blue contours) and returned flow occurrence (white to red isolines). The black line represents the average rainfall over the basin. b) Simulated gravitational moisture (filled green-to-blue contours) and runoff (yellow-to-red isolines). The black line represents streamflow at the outlet of the basin. The green-to-blue color bar serves as a reference for capillary moisture and gravitational water content.

4.2 Flash flood processes

Figure 13 presents the proposed 2D diagrams obtained for the simulation of the La Liboriana basin flash flood using a spatial discretization with 50 groups. Figure 13a includes the evolution of the average rainfall over the basin (black line), and the spatiotemporal evolution of capillary storage (filled isolines) and return flow (colored isolines from white to red) by groups. For the analysis, it is relevant to highlight that higher numbered groups are located away from the outlet of the basin and correspond in this case to considerably steeper slopes. Figure 13b presents the evolution of streamflow at the outlet of the basin (black line), as well as the gravitational storage (filled isolines) and runoff (colored isolines) spatiotemporal evolution. Figure 13 shows variations in the capillary and gravitational storages associated with Event 1 in the higher numbered groups. The capillary storage remains high in almost all the basin until the start of Event 2. According to the conceptualization of the model, the gravitational storage and surface runoff start to interact when the capillary storage is full. In this case, this situation is set up by Event 1. The model runs for Event 2 using dry initial states, ~~showing~~ ~~show~~ no flooding in the results.

The temporal variability of rainfall intensity plays an important role in the hydrograph structure. During Event 1, rainfall accumulated over the basin at a relatively stable rate (Figure 14a). On the other hand, Event 2 presents a significant increase in rainfall rate in the second half of the life cycle (Figure 14b). This change in precipitation intensity is associated with a considerable ~~intensification~~ ~~enhancement~~ of the training convective cores due to orographic effects. Events 1 and 2 also exhibit differences in the elapsed time between rainfall occurrence and streamflow increment given the relative timing of stratiform versus convective rainfall (see the gray band in Figure 14a and b). We compute the elapsed time between the rainfall and the simulated streamflow by measuring the time

680 differences between the lines for the cumulative rainfall and streamflow in Figure 14. For Event 1, the median elapsed time between rainfall and streamflow (Et_{p50}) is 1.12 hours, while for Event 2, Et_{p50} is 0.79 hours. The median elapsed time between the convective portion and the streamflow (Etc_{p50}) in Event 1 is 0.75 and 0.46 in Event 2. The minimum value of the convective elapsed time Etc_{min} also descends from 0.42 to 0.25 hours. On the other hand, there is an increase in
685 median elapsed time between stratiform rainfall and streamflow (Ets_{p50}) from 1.21 to 1.83 hours. The observed differences are largely ~~by due to~~ the timing of the convective precipitation during each of the events. During Event 1, the convective precipitation occurred near the end of the event, explaining the delayed peak discharge time (see Figure 5).

According to Figure 14b ~~for Event 2~~, the accumulations of streamflow runoff and convective
690 rainfall become similar with the increase in time. ~~Additionally, the runoff has a lag and shows signs of attenuation of the convective signal. However, this description~~ ~~This fact highlights the strong control that, in this case, the convective portion has on the runoff, with almost no effect of the stream network filtering out the convective signal, most likely due to the size and the rapid response of the basin.~~ ~~This description, however,~~ only applies for the runoff portion, since the evolution is different when
695 we consider the total simulated streamflow.

4.3 Landslide and flood simulations

Figure 15a presents the observed landslides triggered by Event 2 based on aerial photos and satellite images (~~Landsat/Copernicus and Google~~) taken before and after the flash flood. Figure 15b shows, by hills, the map of total unstable cells during the simulation period, and Figure 15c shows the time
700 series of the number of simulated unstable cells during Event 2 (continuous purple line) and the mean rainfall over the basin (inverse axes, blue line). Calibration of the landslide ~~model submodel~~ was performed by finding the maximum overlap between simulated and observed unstable and stable cells, and at the same time reducing the overall number of false positives and false negatives. It is important to note that the calibration strategy is not a cell-by-cell modification of the parameters involved but rather a basin-wide modification of soil properties. A sensitivity analysis of soil
705 parameters is carried out by making small variations of the variables within specified intervals: ϕ between 25 and 32, γ between 17 and 19, C' between 3.5 and 4.2, and Z between 0.1 and 3 ~~mm~~. The sensitivity analysis suggests that slight variations in the parameter in Z produce ~~significant the largest~~ changes in the ~~results, with overestimation of the~~ number of unstable cells ~~or no unstable~~
710 ~~cells at all~~. Following Table 1, the average soil depth in the basin is only 0.3 m, a value that ~~likely~~ corresponds to underestimation according to the inspections during field visits. For this reason, the results presented in Figure 15 use a Z map scaled by a calibration factor of 3.5, preserving the spatial dependence on the slope but achieving a more realistic soil depth and better spatial distribution of a landslide occurrence.

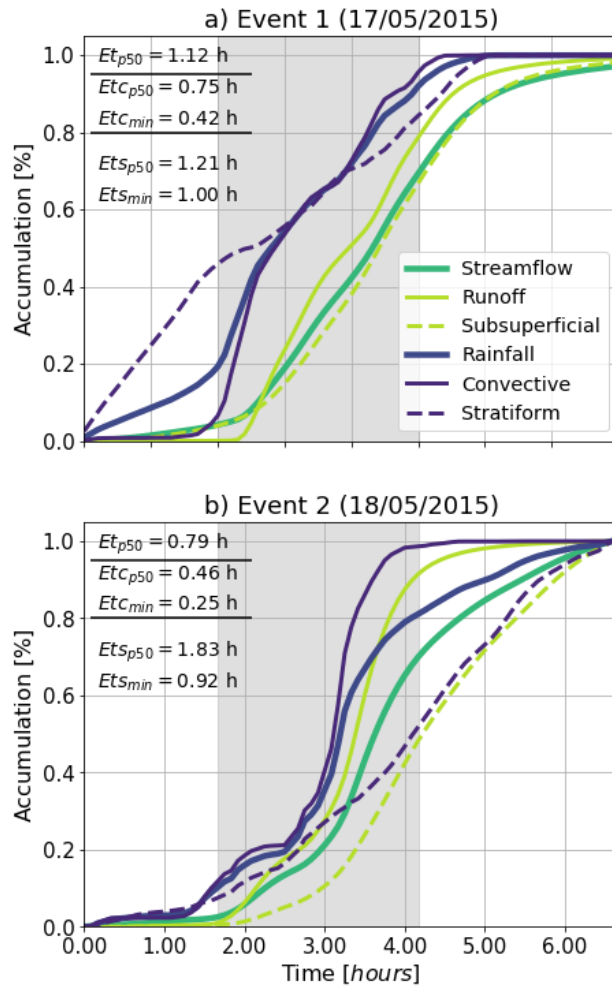


Figure 14. Accumulated rainfall and streamflow for a) Event 1 and b) Event 2. The accumulation is expressed in percentage with respect to the total value in each case. The median elapsed time and minimum elapsed time \ominus are estimated between total (Et_{p50} , Et_{min}), convective ($Et_{c_{p50}}$, $Et_{c_{min}}$), and stratiform ($Et_{s_{p50}}$, $Et_{s_{min}}$) rainfall and the runoff portion of the streamflow. Gray bands correspond to the periods for elapsed time estimation.

715 a) Observed landslides triggered by Events 1 and 2. The figure is based on aerial photos and satellite images (Landsat/Copernicus, and images available on Google) taken before and after the flash-flood event. b) Map of total unstable cells during the simulation period. c) Time series of the number of simulated unstable cells during Event 2 (continuous purple line) and mean rainfall over the basin (inverse axes, blue line).

720 The model represents the spatial distribution of the areas that are prone to trigger shallow landslides during Event 2 reasonably well, especially in the upper part of the basin, showing a significant density of unstable cells in the hills where slides took place. This result is important because in

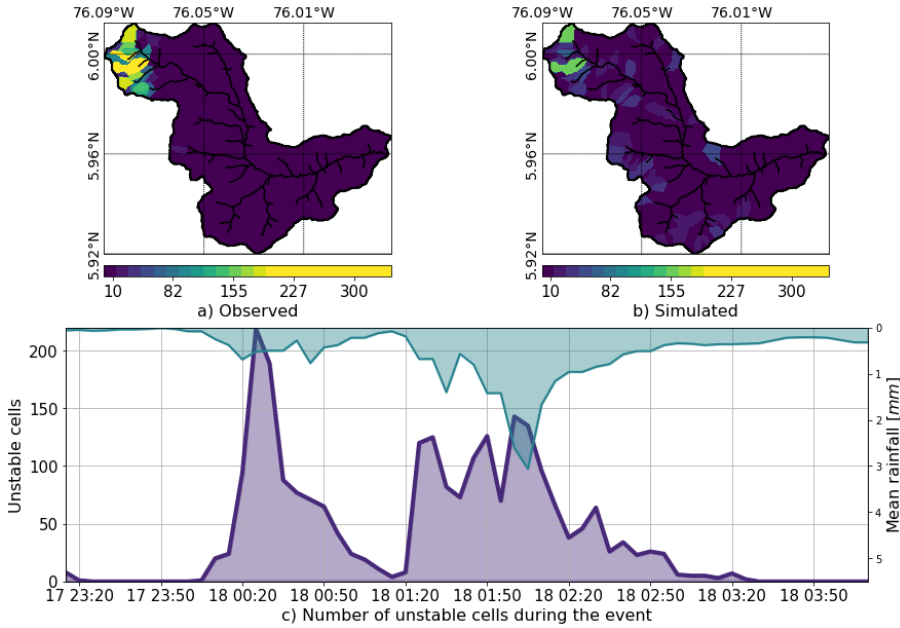


Figure 15. a) Observed landslides triggered by Events 1 and 2. The figure is based on aerial photos and satellite images taken before and after the flash flood event. b) Map of total unstable cells during the simulation period. c) Time series of the number of simulated unstable cells during Event 2 (continuous purple line) and mean rainfall over the basin (inverse axes, blue line).

that sense, it serves to verify the capability of the model to estimate risk areas only considering topography and rainfall data. On the other hand, there are some false positives in the middle of the basin, which could be related to the poor description of the soils. The landslide model has been used in a nearby watershed with similar characteristics, but with high-quality distributed information (Aristizábal et al., 2016). In that case, the model shows a better performance, which highlights the relevance of the input data. A pinpoint localization of the unstable cells is still considered a hard task, in part due to the small temporal and spatial scale at which landslide processes take place (Aristizábal et al., 2016; Dhakal and Sidle, 2004; Wu and Sidle, 1995). Notwithstanding the difficulties, the results suggest that the model simulations could have been used and should be used in the future for early detection and warning to improve both short- and long-term risk reduction strategies.

Figure 16 shows the identification of the flood spots at the peak of Event 2 (May 18, 2015, 2:00 a.m.) as simulated using HydroFlash. Figures 16b to f present a detailed view of the results from the outlet of the basin to the upper region. Cases presented in Figures 16e and f exhibit a satisfactory agreement with observed flood spots (blue shadow). Cases in Figures 16c and d also show a good approximation, but with minor spatial shifts in some sections. The largest spatial differences are observed in Figures 16b. At the entrance of the urban zone, the model overestimates the flood spots. The model results indicate that 11% of flood spots occur at elements of order 1 and 2, and 18, 38 and

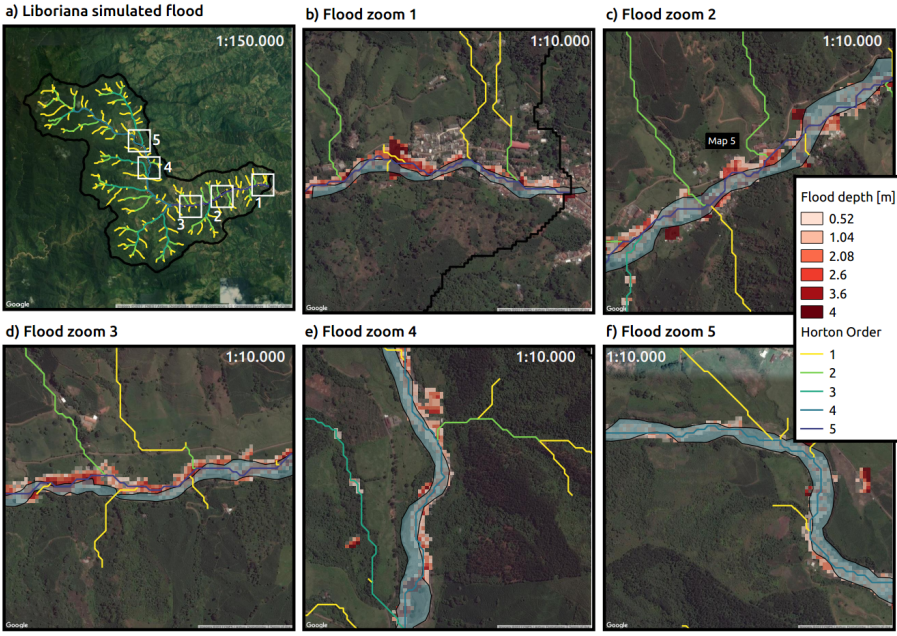


Figure 16. Simulated flood spot at the peak of Event 2 in different locations. a) Basin drainage network. White squares correspond to regions of interest highlighted in panes b) to f). The colors of the streams correspond to the Strahler order of the network. b) Zoom at the outlet of the basin, where an important portion of the human and infrastructure losses took place. c) Zoom at La Margarita settlement also affected by the flash flood. d) to f) Zoom at key locations along the principal stream. Observed flood spots are shown in blue polygons and model flood spots in red to white grids.

740 32% occur at orders 3, 4 and 5, respectively. Table 4 summarizes the described percentages and the total length of each order. These results also highlight a coherent geomorphological representation of the flooded channels and hills relative to the order.

Table 4. Channels and flooded cells percentages summary. Sh_0 and Ss_0 correspond to the mean hill and stream slope, respectively. L corresponds to the total channel length. F Spots and S spots correspond to the flooded and slides percentages, respectively.

Order	Sh_0 [%]	Ss_0 [%]	L [km]	F Spots	Ss Spots
1	60	37	59	5	64.5
2	57	27	26	6	26.3
3	49	13	16	18.5	5.5
4	43	9	10	38.5	3.6
5	42	6	6	32	0.05
Mean/total	50	18	117	100	100

5 Discussion

On the morning of May 18, 2015, a flash flood occurred in the steep La Liboriana basin, in the mu-
745 nicipality of Salgar, Department of Antioquia, Colombia, leaving more than 100 human casualties, 535 houses destroyed, and significant infrastructure loses. Due to the lack of local information of soil type, land use and real-time hydrometeorological data, the La Liboriana case implies a challenge for flash flood prediction, modeling and, consequently, risk management. The present paper introduces a [hydrologic-hydrological](#) model-based approach and an integral graphical analysis tool
750 (an integrated spatiotemporal analysis of rainfall evolution, together with soil storages in the basin) for the following purposes: 1) to simulate and understand the soil-rainfall-discharge processes that led to the 2015 Salgar flash flood, and 2) to propose it as a radar QPE-based and modeling-based landslide and flash flood guidance low-cost tool for basins with scarce data and regions with limited resources.

755 The methodology implies [the development of a distributed hydrologic model with the capabilities of changes and additions to the TETIS distributed hydrological model including](#) tracking independently convective and stratiform precipitation within the model, as well as keeping track of the runoff and subsurface portions of the streamflow. [TETIS was](#) coupled with a shallow landslide submodel and HydroFlash, a one-dimensional [flash-flood-floodplain](#) scheme. The model proposed here indeed
760 allows studying the different hydrological processes relevant to flash flood and landslide occurrence by using different simulation resources, serving as the basis for a better understanding of the overall basin response. [Despite the lack of data, the evidence suggest that the results represents, to a large degree, the magnitude of the disaster; considering also that the simulated peak flow is consistent with the peak flow envelope proposed by Gaume et al. \(2009\) for flash floods.](#) This approach helps to examine [the first-order](#) flood-generating mechanisms or causative factors both in time and in space, focusing on the [most](#) important physical processes (Klemes, 1993; Merz and Blöschl, 2003). [It is hoped that knowledge improvement leads to, potentially allowing](#) the anticipation of [warning](#) [flash flooding events, the issue of warnings](#), and response by risk management entities.

770 The evolution of the simulation of Events 1 and 2 show evidence of remarkable behavioral differences. During Event 1, both gravitational and capillary tanks are filled along and across the basin as a result of the quasi-homogeneous rainfall spatial distribution ([Zoccatelli et al., 2011](#)). [Zoccatelli et al. \(2011\) found similar results for watersheds in Europe with areas ranging between 982 and 52 km².](#) The return flow is low, and most of the runoff occurs within the first 20 groups (40% of the watershed closest to the outlet). In the period between both events, there is a recession in the capillary and gravitational storages in the entire basin. Capillary storage decays considerably slower than gravitational storage. During Event 2, the flash flood triggering event, the first convective core saturates both capillary and gravitational storages in the upper part of the basin and generates both return flow and significant runoff. Due to soil saturation, the second convective core results mainly in surface runoff. During this event, extreme runoff rates are evident in the up-
775

780 per part of the basin, collocated with the steeper slopes. On the other hand, subsurface flow is
781 more important in magnitude than runoff describing Event 1, while runoff is more relevant for
782 Event 2. The precedent storage and the presence of thunderstorm training profoundly condition
783 the streamflow during Event 2. The overall evidence suggests that precedent capillary moisture in
784 the basin plays an essential role in modulating river discharge. This behavior could be linked to
785 the temporal occurrence and relative importance and timing of stratiform and convective formations
786 previously described. During the extreme event, when the soils were already wet, the convective
rainfall fraction dominated the hydrograph formation. While stratiform rainfall plays an important
role moistening the entire basin, convective rainfall generates considerable runoff, leading to flash
flooding. Several authors have argued about the role of convective rainfall triggering flash floods
787 (Doswell et al., 1996; Kahana et al., 2002; Schumacher and Johnson, 2005; Delrieu et al., 2005; Šálek et al., 2006; Milelli et al., 2006;
however, to our knowledge no other study has tracked convective and stratiform water in a modeling
setting to explore their relative role leading to flash flooding.

788 While convective and stratiform partitioning ~~could~~ influence the runoff and subsurface flow separation,
789 the spatial distribution of rainfall relative to watershed network morphometry structure
790 ~~impose~~also imposes a condition on the hydrological response of the basin (Douinot et al., 2016). In
791 other words, hydrograph formation is determined not only by the rainfall accumulation or maximum
792 intensity but also by its spatial structure (Zoccatelli et al., 2011; Douinot et al., 2016). As men-
793 tioned before, average rainfall accumulation over the basin for Events 1 and 2 is 47 ~~mm~~mm and 38
794 ~~mm~~mm, respectively. During ~~Event~~Events 1 ~~(and~~2), convective (stratiform) average accumulations
795 are 28 (23) and 17 (14) ~~mm~~mm, respectively. The maximum rainfall intensities are relatively similar
796 with 150 ~~mm/h~~mm and 180 ~~mm/h~~mm for Events 1 and 2, respectively, but the location was
797 significantly different. Convective rainfall occurrence at the upper subbasins has significant impli-
798 cations due to geomorphological conditions associated to zero-order subbasins (Sidle et al., 2018).
799 Besides, at Event2 with a moist soil, the convective portion of the rainfall significantly influences the
800 hydrograph formation. Additionally, when we compare Events 1 and 2, there is an interplay between
801 the ~~rain~~rainfall spatial structure and the soil storage capacity. During Event 1, there is almost no
802 saturation, hence runoff production is low, while Event 2 is influenced by the pre-event water and
803 the occurrence of multiple convective systems over the same region. The structure of the rainfall as-
804 sociated with the La Liboriana event and its interaction with the soils highlights the need to consider
805 in more detail the role of orographic rainfall intensification in practical applications such as early
806 warning systems. Evidence suggests the spatial structure of the rainfall is at least as important as the
807 geomorphological features of the basin in regulating the generation of flash flood events.

808 An integrated spatiotemporal analysis of rainfall evolution, together with soil storages in the basin,
809 is necessary to study the relevance of antecedent conditions and precipitation type, intensity, and
810 location in the generation of flash flood events. Event 1 increased the overall soil moisture with an
811 associated decrease in infiltration rates, similar to the results reported by Marchi et al. (2010); Penna

et al. (2011) and Zehe et al. (2010); additionally, low infiltration increased the runoff rates, ultimately affecting the susceptibility of the basin to flash flood occurrence (Wagner et al., 1999; Penna et al., 2011; Tramblay et al., 2012). Due to geomorphological characteristics (see Table 4), water tends to 820 reach faster the channels in hills of order 1 and 2, and, at the same time, the sediment production and transport in these hills tend to be larger. Order 3 subbasins most likely act as transport elements, with no important energy losses (Table 4), and floods tend to occur at order 4 and 5 subbasins due to the widening of the channel and slope attenuation.

Different authors have focused on trying to understand the general causative factors behind the 825 occurrence of flash floods (Marchi et al., 2010), ~~finding results similar to ours, with a significant role of considering also suggesting a significant combined role of~~ geomorphology, orography, ~~soil characteristics~~ and local convection. For example, Lehmann and Or (2012), using a shallow landslide model, ~~finds found~~ an important role of the topography and the rainfall conditions. Turkington et al. (2014) ~~shows showed~~ how intense locally driven convection ~~appears to be is~~ the main meteorological 830 trigger for flash occurrence in the French Alps. Camarasa-Belmonte (2016) ~~shows how showed the important role of~~ rainfall intensity and duration ~~influences on~~ the shape of the hydrograph, with intense rainfall shortening the response time of the basin, and large durations increasing the flood peak. In the Mediterranean region, Boudou et al. (2016) ~~states stated~~ that in addition to the rainfall, 835 geomorphological characteristics and antecedent soil conditions are key in the generation of flash flooding.

The landslides submodel presents an overall acceptable performance with limitations in certain 840 regions. In particular, there are some false positives in the middle of the basin. These limitations could be associated with the assumptions and approximations inherent to the submodel, including that it only determines unstable cells by slowly filling the soil matrix with water, which, in this case, given the lack of information, depends on the soil depth derived from the topography, and that the model does not consider instability due to intense rainfall events. The lack of detailed soil depth information could explain the false positives landslides. On the other hand, the relation between landslides and high-intensity rainfall must be explored and included in this kind of models. There is also an apparent contradiction regarding the depth of the soils in the basin: While the 845 values derived from topography appear to work well for the hydrological model, the depth had to be calibrated to obtain a better representation of landslides. There are two possible explanations for the contradiction, (i) that the soils are in fact thicker in the entire basin, but the calibration of the infiltration and percolation rates corrected the hydrological simulations, and (ii) that the landslides submodel is too simplistic, or that no other parameters were calibrated, possibly resulting in over 850 calibration of the soil depth. This is an aspect that needs to be explored further.

The landslide submodel has been used in a nearby watershed with similar characteristics, but with high-quality distributed information (Aristizábal et al., 2016). In that case, the model shows a better performance, which highlights the relevance of the quality of the input data. It is also

important to consider that, a pinpoint localization of the unstable cells is still considered a hard task, in part due to the small temporal and spatial scale at which landslide processes take place (Aristizábal et al., 2016; Dhakal and Sidle, 2004; Wu and Sidle, 1995).

Similarly, results of the HydroFlash submodel are satisfactory despite the hydraulic over simplifications, and are potentially useful for issuing warnings to the community. From that point of view, it is important to stress that the low computing cost of HydroFlash, different to that of detailed 2D/3D hydraulic geomorphological models, makes it possible to be executed in real time coupled with rainfall observations, providing valuable information that, while not 100% accurate spatially, helps discriminating to a high degree, for example, which communities need to be evacuated given an extreme event. In addition, the floodplain submodel provides an indirect estimation of the sediment load during extreme events. In the 2015 Salgar simulations, the peak discharge obtained with the hydrological model was $220 \text{ m}^3 \text{s}^{-1}$; the total streamflow considering the sediment load reached values around $285 \text{ m}^3 \text{s}^{-1}$, for a $Q_{\text{sed}}/Q_{\text{sim}}$ ratio of 1.3. The extra 30% discharge corresponding to the sediment load is certainly a relevant contribution to the total discharge, with impacts in the floodplain determination. Considering the stream network slope, the simulated ratio is comparable with reports in the literature Rickenmann and Koschni (e.g. 2010). The sediment load is mainly constrained by the maximum sediment concentration C_{max} and the depth of the flow, suggesting that better information about C_{max} could improve the simulation of flood spots.

However useful, the evidence in this work only takes into account two successive events; an analysis of more cases and different spatial scales (different basins) would provide robust conclusions in this direction. It is clear that focusing on a single extreme event, rather than on a spectrum of floods, is not conclusive enough Merz and Blöschl (2003). The model simulation results suggest it is imperative to study in depth the long-term link between the relative basin and drainage network orientation and the preferred path of precipitation events and its role in defining the frequency of flash flood occurrence. A better understanding of the network-hills-preferential rainfall advection structure could provide information about basins prone to flash floods when information is scarce.

880 6 Conclusions

Extreme rainfall events such as the one that triggered the La Liboriana tragedy frequently take place in Colombia and the entire global tropical belt over ungauged basins, often triggering flash floods and debris flows, which endanger vulnerable communities due to poor long-term planning and lack of functional early warning systems. There is a global need for better knowledge and understanding of the hydrological and meteorological conditions that, combined, lead to the manifestation of disasters linked to natural hazards. Such an understanding must result in useful practical applications that improve risk management practices and thus save lives. In the current work, we approach the problem from a hydrological modeling point of view, trying, despite the data limitations and the un-

certainty of the results, to shed some light on the first-order processes that modulate the occurrence
890 of flash floods in the region of study.

In the case of the La Liboriana flash flood, radar reflectivity fields were available from a C-Band
radar operated by the Early Warning System of Medellín and its metropolitan area, as part of a
local risk management strategy. While the municipality of Salgar is located far from Medellín's
metropolitan area, the radar is approximately 90 km away from Salgar, and the reflectivity retrievals
895 enable the classification of precipitation fields into convective and stratiform areas, using widely
accepted methodologies by the meteorological community. Radar reflectivity also serves as a proxy
for precipitation, allowing a quantitative estimation of rainfall fields. This estimation was used to-
gether with the [hydrologie-TETIS](#) model to assess the different basin-wide processes taking place
during the flash flood triggering rainfall event. The limitations of the methodology presented in this
900 work do not allow representing all the detailed small-scale preferential pathways of the water in
the watershed, but rather focus on the first-order processes to study the partitioning between runoff
vs. subsurface flow. Additionally, the model results are used to obtain a conceptual idea about the
general processes, but it must be taken into account that the simulations are subject to a calibration
process that could lead to erroneous conclusions about the mentioned processes. This consideration
905 could be true even [when considering that](#) different steps were taken trying to avoid this situation.

The overall model simulation methodology reproduces the estimated magnitude and reported tim-
ing of the La Liboriana flash flood discharge peak quite well, showing robustness to changes in the
most important model parameters. Simulation results suggest that the soil storage capacity available
before flooding event, impacted not only the flood magnitude itself, but also the response time of the
910 catchment, highlighting the role of soil wetness distribution within the basin. The model also repro-
duces the areas of regional landslide occurrence and flood spot locations satisfactorily. The model
simulation results indicate that the flash flood and the regional landslide features were strongly in-
fluenced by the observed antecedent rainfall associated with a northwesterly stratiform event that
recharged the gravitational and capillary storages in the entire basin. The [hydrological-TETIS](#) model
915 simulation shows that the antecedent event set wet conditions in the entire basin before the occur-
rence of the flash flood event, governing the streamflow during the latter. The results of the model
simulation also suggest that the first of the two successive convective cores (training convective el-
ements) over the same region during the second precipitation event (the flash flood event) saturated
both capillary and gravitational storages in the upper part of the basin and generated both return
920 flow and significant runoff. The second convective core resulted mainly in surface runoff spatially
collocated with the steeper slopes, generating the kinetic energy needed to produce the La Liboriana
flash flood. The overall results also show a good agreement between the simulated flood spots and
the observed ones, despite the limitations imposed by the resolution of the DEM used for extracting
cross-sections and the model oversimplifications.

925 Results of the landslide submodel and HydroFlash, while satisfactory, are far from perfect, showing significant differences compared to observations ~~when compared in the detail~~. The evidence suggests, by and large, that most of the observed differences are mainly due to the lack of higher spatial resolution DEM, in the case of HydroFlash, and due to the lack of a detailed soil dataset, in the case of the landslide submodel. However, there is also considerable room for improvement in both
930 submodels, including a better representation of non-Newtonian hydraulic processes in HydroFlash, and a direct link between landslides and flood spots following, for example, a similar strategy to the one presented in the STEP-TRAMM model (Fan et al., 2017). Notwithstanding the difficulties, the results suggest that the submodel simulations could have been used and should be used in the future for early detection and warning to improve both short- and long-term risk reduction strategies.

935 Considering all the shortcomings and generalizations, the described model-based approach is potentially useful to assess flood-generating mechanisms and as a tool for policy-makers, not only for short-term decisions in the context of an early warning system but also as a planning resource for long-term risk management. The results suggest it is possible to use low-cost methodologies such as the one introduced here as a risk management tool in countries and regions with scarce resources.

940 7 Acknowledgments

This work was supported by SIATA (Sistema de Alerta Temprana de Medellín y el Valle de Aburrá) funds provided by Área Metropolitana del Valle de Aburrá (AMVA), Municipio de Medellín, Grupo EPM, and ISAGEN under the Research and Technology Contract CD511, 2017. Universidad Nacional de Colombia partly funded Nicolás Velásquez under the Facultad de Minas graduate scholarship program. Both authors would like to thank anonymous reviewer 1 for the detailed and insightful comments that helped to clarify and highlight the message of this work. Both authors also thank Dr. Eric Gaume, reviewer 2, for his thoughtful comments.

945 For the technically inclined reader, the ~~hydrologic~~ TETIS hydrological model and submodels are written in Fortran 90, and the interface to the model, pre-process, and post-process tools are in
950 Python 2.7. The Fortran code is warped to Python using **f2py** (Peterson, 2009), and it is publicly available under the Watershed Modeling Framework **WMF** in a web repository (**GitHub**).

Appendix A: Figures

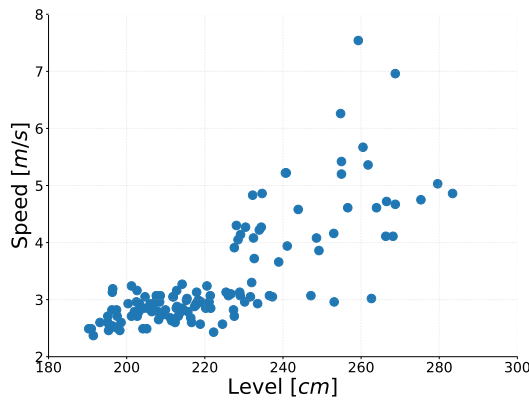


Figure A.1. Scatter plot of water level (depth) (cm) and surface speed (ms^{-1}) for Doña Marfa basin, located in the Aburrá Valley (Basin outlet coordinates: 75.651°W, 6.190°N). The basin slope is 34.09%, the area :72.84 km^2 , and the maximum (minimum) height is 2,835 m.a.s.l. (1,562 m.a.s.l.)

References

Adamovic, M., Branger, F., Braud, I., and Kralisch, S.: Development of a data-driven semi-distributed hydrological model for regional scale catchments prone to Mediterranean flash floods, *Journal of Hydrology*, 541, 173–189, doi:10.1016/j.jhydrol.2016.03.032, <http://dx.doi.org/10.1016/j.jhydrol.2016.03.032>, 2016.

Aristizábal, E., Vélez, J. I., Martínez, H. E., and Jaboyedoff, M.: SHIA_Landslide: a distributed conceptual and physically based model to forecast the temporal and spatial occurrence of shallow landslides triggered by rainfall in tropical and mountainous basins, *Landslides*, 13, 497–517, doi:10.1007/s10346-015-0580-7, 2016.

Aronica, G. T., Brigandí, G., and Morey, N.: Flash floods and debris flow in the city area of Messina, north-east part of Sicily, Italy in October 2009: The case of the Giampilieri catchment, *Natural Hazards and Earth System Science*, 12, 1295–1309, doi:10.5194/nhess-12-1295-2012, 2012.

ASF, J.: Dataset: ASF DAAC 2015, ALOS PALSAR Radiometric Terrain Corrected high res; Includes Material JAXA/METI 2007, doi:10.5067/Z97HFCNKR6VA, <https://vertex.daac.asf.alaska.edu/>, 2011.

Baltaci, H.: Meteorological analysis of flash floods in Artvin (NE Turkey) on 24 August 2015, *Natural Hazards and Earth System Sciences*, 17, 1221–1230, doi:10.5194/nhess-17-1221-2017, <https://www.nat-hazards-earth-syst-sci.net/17/1221/2017/>, 2017.

Berne, A. and Krajewski, W.: Radar for hydrology: Unfulfilled promise or unrecognized potential?, *Advances in Water Resources*, 51, 357 – 366, doi:<https://doi.org/10.1016/j.advwatres.2012.05.005>, <http://www.sciencedirect.com/science/article/pii/S0309170812001157>, 35th Year Anniversary Issue, 2013.

Beven, K.: Kinematic subsurface stormflow, *Water Resources Research*, 17, 1419–1424, doi:10.1029/WR017i005p01419, 1981.

Beven, K.: Towards integrated environmental models of everywhere: uncertainty, data and modelling as a learning process, *Hydrology and Earth System Sciences*, 11, 460–467, doi:10.5194/hess-11-460-2007, <http://www.hydrol-earth-syst-sci.net/11/460/2007/>, 2007.

Bisht, S., Chaudhry, S., Sharma, S., and Soni, S.: Assessment of flash flood vulnerability zonation through Geospatial technique in high altitude Himalayan watershed, Himachal Pradesh India, *Remote Sensing Applications: Society and Environment*, 12, 35–47, doi:10.1016/j.rsase.2018.09.001, <https://doi.org/10.1016/j.rsase.2018.09.001>, 2018.

980 Blöschl, G., Sivapalan, M., Wagener, T., Viglione, A., and Savenije, H.: Runoff Prediction in Ungauged Basins, in: *Runoff Prediction in Ungauged Basins: Synthesis across Processes, Places and Scales*, edited by Blöschl, G., Sivapalan, M., Wagener, T., Viglione, A., and Savenije, H., Cambridge University Press, Cambridge, [https://www.cambridge.org/core/books/runoff-prediction-in-ungauged-basins/A5DFE99C3CA857127C4C03C6C20032EE](https://www.cambridge.org/core/books/runoff-prediction-in-ungauged-basins/runoff-prediction-in-ungauged-basins/A5DFE99C3CA857127C4C03C6C20032EE), 2012.

985 Bonell, M., McDonnell, J. J., Scatena, F. N., Seibert, J., Uhlenbrook, S., and van Lanen, H. A. J.: HELP-ing FRIENDs in PUBs: Charting a course for synergies within international water research programmes in gauged and ungauged basins, *Hydrological Processes*, 20, 1867–1874, doi:10.1002/hyp.6196, 2006.

990 Borga, M., Anagnostou, E. N., Blöschl, G., and Creutin, J. D.: Flash flood forecasting, warning and risk management: The HYDRATE project, *Environmental Science and Policy*, 14, 834–844, doi:10.1016/j.envsci.2011.05.017, 2011.

Boudou, M., Lang, M., Vinet, F., and C??ur, D.: Comparative hazard analysis of processes leading to remarkable flash floods (France, 1930??1999), *Journal of Hydrology*, 541, 533–552, doi:10.1016/j.jhydrol.2016.05.032, <http://dx.doi.org/10.1016/j.jhydrol.2016.05.032>, 2016.

995 Bruni, G., Reinoso, R., Van De Giesen, N. C., Clemens, F. H. L. R., and Ten Veldhuis, J. A. E.: On the sensitivity of urban hydrodynamic modelling to rainfall spatial and temporal resolution, *Hydrology and Earth System Sciences*, 19, 691–709, doi:10.5194/hess-19-691-2015, 2015.

Camarasa-Belmonte, A. M.: Flash floods in Mediterranean ephemeral streams in Valencia Region (Spain), *Journal of Hydrology*, doi:10.1016/j.jhydrol.2016.03.019, 2016.

1000 Castillo, V. M., Gómez-Plaza, A., and Martínez-Mena, M.: The role of antecedent soil water content in the runoff response of semiarid catchments: A simulation approach, *Journal of Hydrology*, 284, 114–130, doi:10.1016/S0022-1694(03)00264-6, 2003.

Chapra, S. C.: *Applied Numerical Methods with MATLAB*, McGraw-Hill, 3rd edn., 2012.

Delrieu, G., Nicol, J., Yates, E., Kirstetter, P.-E., Creutin, J. D., Anquetin, S., Obled, C., Saulnier, G.-M., 1005 Ducrocq, V., Gaume, E., Payrastre, O., Andrieu, H., Ayral, P.-A., Bouvier, C., Neppel, L., Livet, M., Lang, M., du Châtelet, J. P., Walpersdorf, A., and Wobrock, W.: The Catastrophic Flash-Flood Event of 8–9 September 2002 in the Gard Region, France: A First Case Study for the Cévennes–Vivarais Mediterranean Hydrometeorological Observatory, *Journal of Hydrometeorology*, 6, 34–52, 2005.

Dhakal, A. S. and Sidle, R. C.: Distributed simulations of landslides for different rainfall conditions, *Hydrological Processes*, 18, 757–776, doi:10.1002/hyp.1365, 2004.

Doswell, C. A., Brooks, H. E., and Maddox, R. A.: Flash Flood Forecasting: An Ingredients-Based Methodology, *Weather and Forecasting*, 11, 560–581, doi:10.1175/1520-0434(1996)011<0560:FFFAIB>2.0.CO;2, [https://doi.org/10.1175/1520-0434\(1996\)011<0560:FFFAIB>2.0.CO;2](https://doi.org/10.1175/1520-0434(1996)011<0560:FFFAIB>2.0.CO;2), 1996.

1010 Douinot, A., Roux, H., Garambois, P. A., Larnier, K., Labat, D., and Dartus, D.: Accounting for rainfall systematic spatial variability in flash flood forecasting, *Journal of Hydrology*, 541, 359–370, doi:10.1016/j.jhydrol.2015.08.024, <http://dx.doi.org/10.1016/j.jhydrol.2015.08.024>, 2016.

1020 Duan, Q., Schaake, J., Andreassian, V., Franks, S., Goteti, G., Gupta, H., Gusev, Y., Habets, F., Hall, a., Hay, L., Hogue, T., Huang, M., Leavesley, G., Liang, X., Nasonova, O., Noilhan, J., Oudin, L., Sorooshian, S., Wagener, T., and Wood, E.: Model Parameter Estimation Experiment (MOPEX): An overview of science strategy and major results from the second and third workshops, *Journal of Hydrology*, 320, 3–17, doi:10.1016/j.jhydrol.2005.07.031, 2006.

Fan, L., Lehmann, P., Mc Ardell, B., and Or, D.: Linking rainfall-induced landslides with debris flows runout patterns towards catchment scale hazard assessment, *Geomorphology*, 280, 1–15, doi:10.1016/j.geomorph.2016.10.007, <http://dx.doi.org/10.1016/j.geomorph.2016.10.007>, 2017.

1025 Foster, G., Huggins, L., and L.D., M.: A Laboratory Study of Rill Hydraulics: I. Velocity Relationships, American Society of Agricultural and Biological Engineers, 3, 0790–0796, doi:10.13031/2013.32873, 1984.

Fragoso, M., Trigo, R. M., Pinto, J. G., Lopes, S., Lopes, a., Ulbrich, S., and Magro, C.: The 20 February 2010 Madeira flash-floods: Synoptic analysis and extreme rainfall assessment, *Natural Hazards and Earth System Science*, 12, 715–730, doi:10.5194/nhess-12-715-2012, 2012.

1030 Francés, F., Vélez, J. I., and Vélez, J. J.: Split-parameter structure for the automatic calibration of distributed hydrological models, *Journal of Hydrology*, 332, 226–240, doi:10.1016/j.jhydrol.2006.06.032, 2007.

Garambois, P. a., Roux, H., Larnier, K., Castaings, W., and Dartus, D.: Characterization of process-oriented hydrologic model behavior with temporal sensitivity analysis for flash floods in Mediterranean catchments, *Hydrology and Earth System Sciences*, 17, 2305–2322, doi:10.5194/hess-17-2305-2013, 2013.

1035 Gaume, E., Bain, V., Bernardara, P., Newinger, O., Barbuc, M., Bateman, A., Blaškovičová, L., Blöschl, G., Borga, M., Dumitrescu, A., Daliakopoulos, I., Garcia, J., Irimescu, A., Kohnova, S., Koutoulis, A., Marchi, L., Matreata, S., Medina, V., Preciso, E., Sempere-Torres, D., Stancalie, G., Szolgay, J., Tsanis, I., Velasco, D., and Viglione, A.: A compilation of data on European flash floods, *Journal of Hydrology*, 367, 70–78, 2009.

1040 Gochis, D., Schumacher, R., Friedrich, K., Doesken, N., Kelsch, M., Sun, J., Ikeda, K., Lindsey, D., Wood, A., Dolan, B., Matrosov, S., Newman, A., Mahoney, K., Rutledge, S., Johnson, R., Kucera, P., Kennedy, P., Sempere-Torres, D., Steiner, M., Roberts, R., Wilson, J., Yu, W., Chandrasekar, V., Rasmussen, R., Anderson, A., and Brown, B.: The great Colorado flood of September 2013, *Bulletin of the American Meteorological Society*, 96, 1461–1487, doi:10.1175/BAMS-D-13-00241.1, 2015.

1045 Golden, L. A. and Springer, G. S.: Channel geometry, median grain size, and stream power in small mountain streams, *Geomorphology*, 78, 64–76, doi:10.1016/j.geomorph.2006.01.031, 2006.

Graham, J.: *Methods of Stability Analysis. Slope Instability*, John Wiley and sons, 1984.

Gruntfest, E. and Handmer, J.: *Coping with Flash Floods*, NATO science series. Partnership sub-series 2, Environmental security, Springer Netherlands, <https://books.google.com.co/books?id=pwsczTbbY9sC>, 2001.

1050 Hardy, J., Gourley, J. J., Kirstetter, P. E., Hong, Y., Kong, F., and Flamig, Z. L.: A method for probabilistic flash flood forecasting, *Journal of Hydrology*, 541, 480–494, doi:10.1016/j.jhydrol.2016.04.007, <http://dx.doi.org/10.1016/j.jhydrol.2016.04.007>, 2016.

Houze, R.: Mesoscale convective systems, *Reviews of Geophysics*, 42, doi:10.1029/2004RG000150, <https://agupubs.onlinelibrary.wiley.com/doi/abs/10.1029/2004RG000150>, 2004.

1055 Houze, R. A., Rasmussen, K. L., Zuluaga, M. D., and Brodzik, S. R.: The variable nature of convection in the tropics and subtropics: A legacy of 16 years of the Tropical Rainfall Measuring Mission satellite, *Reviews of Geophysics*, 53, 994–1021, doi:10.1002/2015RG000488, 2015.

1060 Hoyos, C., Ceballos, L., Pérez, J., Sepúlveda, J., López, S., Zuluaga, M., Velásquez, N., Herrera, L., Hernández, O., Guzmán, G., and Zapata, M.: Meteorological Conditions Leading to the 2015 Salgar Flash Flood: Lessons for Vulnerable Regions in Tropical Complex Terrain, *Natural Hazards and Earth System Sciences Discussions*, 2019, 1–43, 2019.

1065 Jonkman, S.: Global perspectives on loss of human life caused by floods, *NATURAL HAZARDS*, 34, 151–175, doi:10.1007/s11069-004-8891-3, 2005.

1070 Kahana, R., Ziv, B., Enzel, Y., and Dayan, U.: Synoptic climatology of major floods in the Negev Desert, Israel, *International Journal of Climatology*, 22, 867–882, doi:10.1002/joc.766, 2002.

1075 Khosravi, K., Pham, B. T., Chapi, K., Shirzadi, A., Shahabi, H., Revhaug, I., Prakash, I., and Tien Bui, D.: A comparative assessment of decision trees algorithms for flash flood susceptibility modeling at Haraz watershed, northern Iran, *Science of the Total Environment*, 627, 744–755, doi:10.1016/j.scitotenv.2018.01.266, <https://doi.org/10.1016/j.scitotenv.2018.01.266>, 2018.

1080 Kirkby, M. J. and Chorley, R. J.: Throughflow, Overland Flow and Erosion, *International Association of Scientific Hydrology. Bulletin*, 12, 5–21, doi:10.1080/02626666709493533, <http://www.tandfonline.com/doi/abs/10.1080/02626666709493533>, 1967.

1085 Klemes, V.: Probability of extreme hydrometeorological events—A different approach, in *Extreme Hydrological Events: Precipitation, Floods and Droughts*, IAHS Publ, 1993.

1090 Kubota, J. and Sivapalan, M.: Towards a Catchment-Scale Model of Subsurface Small-Scale Process-Based Modelling and Runoff Generation Based on Synthesis of Field Studies, *Hydrological Processes*, 9, 541–554, 1995.

Lehmann, P. and Or, D.: Hydromechanical triggering of landslides: From progressive local failures to mass release, *Water Resources Research*, 48, 1–24, doi:10.1029/2011WR010947, 2012.

Leopold, L.B., M. T.: The hydraulic geometry of stream channels and some physiographic implications, *Geological survey professional paper*, 1953.

Llasat, M. C., Marcos, R., Turco, M., Gilabert, J., and Llasat-Botija, M.: Trends in flash flood events versus convective precipitation in the Mediterranean region: The case of Catalonia, *Journal of Hydrology*, 541, 24–37, doi:10.1016/j.jhydrol.2016.05.040, <http://dx.doi.org/10.1016/j.jhydrol.2016.05.040>, 2016.

Longoni, L., Ivanov, V. I., Brambilla, D., Radice, A., and Papini, M.: Analysis of the temporal and spatial scales of soil erosion and transport in a Mountain Basin, *Italian Journal of Engineering Geology and Environment*, 16, 17–30, doi:10.4408/IJEGE.2016-02.O-02, 2016.

Marchi, L., Borga, M., Preciso, E., and Gaume, E.: Characterisation of selected extreme flash floods in Europe and implications for flood risk management, *Journal of Hydrology*, 394, 118–133, doi:10.1016/j.jhydrol.2010.07.017, <http://dx.doi.org/10.1016/j.jhydrol.2010.07.017>, 2010.

Marchi, L., Cavalli, M., Amponsah, W., Borga, M., and Crema, S.: Upper limits of flash flood stream power in Europe, *Geomorphology*, 272, 68–77, doi:10.1016/j.geomorph.2015.11.005, <http://dx.doi.org/10.1016/j.geomorph.2015.11.005>, 2016.

Marra, F., Destro, E., Nikolopoulos, E. I., Zoccatelli, D., Dominique Creutin, J., Guzzetti, F., and Borga, M.: Impact of rainfall spatial aggregation on the identification of debris flow occurrence thresholds, *Hydrology and Earth System Sciences*, 21, 4525–4532, doi:10.5194/hess-21-4525-2017, 2017.

Martín-Vide, J. P. and Llasat, M. C.: The 1962 flash flood in the Rubí stream (Barcelona, Spain), *Journal of Hydrology*, 566, 441–454, doi:10.1016/j.jhydrol.2018.09.028, <https://doi.org/10.1016/j.jhydrol.2018.09.028>, 2018.

1100 Merz, R. and Blöschl, G.: A process typology of regional floods, *Water Resources Research*, 39, 1–20, doi:10.1029/2002WR001952, <http://doi.wiley.com/10.1029/2002WR001952>, 2003.

Milelli, M., Llasat, M. C., and Ducrocq, V.: The cases of June 2000, November 2002 and September 2002 as examples of Mediterranean floods, *Natural Hazards and Earth System Sciences*, 6, 271–284, doi:10.5194/nhess-6-271-2006, <https://www.nat-hazards-earth-syst-sci.net/6/271/2006/>, 2006.

1105 Norbiato, D., Borga, M., Degli Esposti, S., Gaume, E., and Anquetin, S.: Flash flood warning based on rainfall thresholds and soil moisture conditions: An assessment for gauged and ungauged basins, *Journal of Hydrology*, pp. 274–290, doi:10.1016/j.jhydrol.2008.08.023, 2008.

Obrien, J.S., J. P.: Laboratory analysis of mudflow properties, *Journal of Hydrological Engineering*, 8, 877–887, 1988.

1110 Osorio, H.G., A. S.: Unidades de suelo representativas de la zona cafetera de Colombia, *Federación de Cafeteros de Colombia*, 2008.

Ozturk, U., Wendi, D., Crisologo, I., Riemer, A., Agarwal, A., Vogel, K., López-Tarazón, J. A., and Korup, O.: Rare flash floods and debris flows in southern Germany, *Science of the Total Environment*, 626, 941–952, doi:10.1016/j.scitotenv.2018.01.172, 2018.

1115 Penna, D., Tromp-Van Meerveld, H. J., Gobbi, a., Borga, M., and Dalla Fontana, G.: The influence of soil moisture on threshold runoff generation processes in an alpine headwater catchment, *Hydrology and Earth System Sciences*, 15, 689–702, doi:10.5194/hess-15-689-2011, 2011.

Peterson, P.: F2PY: a tool for connecting Fortran and Python programs, *International Journal of Computational Science and Engineering*, 4, 296, doi:10.1504/IJCSE.2009.029165, <http://www.inderscience.com/link.php?id=29165>, 2009.

1120 Piper, D., Kunz, M., Ehmele, F., Mohr, S., Mühr, B., Kron, A., and Daniell, J.: Exceptional sequence of severe thunderstorms and related flash floods in May and June 2016 in Germany. Part I: Meteorological background, *Natural Hazards and Earth System Sciences Discussions*, pp. 1–30, doi:10.5194/nhess-2016-275, <http://www.nat-hazards-earth-syst-sci-discuss.net/nhess-2016-275/>, 2016.

1125 Poveda, G., Vélez, J. I., Mesa, O. J., Cuartas, A., Barco, J., Mantilla, R. I., Mejía, J. F., Hoyos, C. D., Ramírez, J. M., Ceballos, L. I., Zuluaga, M. D., Arias, P. a., Botero, B. a., Montoya, M. I., Giraldo, J. D., and Quevedo, D. I.: Linking Long-Term Water Balances and Statistical Scaling to Estimate River Flows along the Drainage Network of Colombia, *Journal of Hydrologic Engineering*, 12, 4–13, doi:10.1061/(ASCE)1084-0699(2007)12:1(4), 2007.

1130 Rennó, C. D., Nobre, A. D., Cuartas, L. A., Soares, J. V., Hodnett, M. G., Tomasella, J., and Waterloo, M. J.: HAND, a new terrain descriptor using SRTM-DEM: Mapping terra-firme rainforest environments in Amazonia, *Remote Sensing of Environment*, 112, 3469–3481, doi:10.1016/j.rse.2008.03.018, <http://linkinghub.elsevier.com/retrieve/pii/S003442570800120X>, 2008.

Rickenmann, D. and Koschni, A.: Sediment loads due to fluvial transport and debris flows during the 2005 flood events in Switzerland, 1007, 993–1007, doi:10.1002/hyp.7536, 2010.

Rodriguez-Blanco, M., Taboada-Castro, M., and Taboada-Castro, M.: Rainfall–runoff response and event-based runoff coefficients in a humid area (northwest Spain), *Hydrological Sciences Journal*, 403, 319–329, doi:10.1080/02626669509491418, <http://www.tandfonline.com/action/journalInformation?journalCode=thsj20>, 2012.

Roux, H., Labat, D., Garambois, P. A., Maubourgues, M. M., Chorda, J., and Dartus, D.: A physically-based parsimonious hydrological model for flash floods in Mediterranean catchments, *Natural Hazards and Earth System Science*, 11, 2567–2582, doi:10.5194/nhess-11-2567-2011, 2011.

Rozalis, S., Morin, E., Yair, Y., and Price, C.: Flash flood prediction using an uncalibrated hydrological model and radar rainfall data in a Mediterranean watershed under changing hydrological conditions, *Journal of Hydrology*, 394, 245–255, doi:10.1016/j.jhydrol.2010.03.021, <http://dx.doi.org/10.1016/j.jhydrol.2010.03.021>, 2010.

Ruiz-Villanueva, V., Díez-Herrero, A., Bodoque, J. M., Ballesteros Cánovas, J. A., and Stoffel, M.: Characterisation of flash floods in small ungauged mountain basins of Central Spain using an integrated approach, *Catena*, 110, 32–43, doi:10.1016/j.catena.2013.06.015, <http://dx.doi.org/10.1016/j.catena.2013.06.015>, 2013.

Šálek, M., Brezková, L., and Novák, P.: The use of radar in hydrological modeling in the Czech Republic – case studies of flash floods, *Natural Hazards and Earth System Science*, 6, 229–236, doi:10.5194/nhess-6-229-2006, 2006.

Savage, S. B. and Sayed, M.: Stresses developed by dry cohesionless granular materials sheared in an annular shear cell, *Journal of Fluid Mechanics*, 142, 391–430, doi:10.1017/S0022112084001166, 1984.

Schumacher, R. S. and Johnson, R. H.: Organization and Environmental Properties of Extreme-Rain-Producing Mesoscale Convective Systems, *Monthly Weather Review*, 133, 961–976, doi:10.1175/MWR2899.1, <http://journals.ametsoc.org/doi/abs/10.1175/MWR2899.1>, 2005.

Seibert, J. and Beven, K. J.: Gauging the ungauged basin : how many discharge measurements are needed?, *Hydrology and Earth System Sciences*, 13, 883–892, doi:10.5194/hessd-6-2275-2009, <http://www.hydrol-earth-syst-sci.net/13/883/2009/>, 2009.

Sepúlveda, J. and Hoyos, C. D.: Disdrometer-based C-Band Radar Quantitative Precipitation Estimation (QPE) in a highly complex terrain region in tropical Colombia., AGU Fall Meeting Abstracts, 2017.

Sepúlveda, J.: Estimación cuantitativa de precipitación a partir de la información de Radar Meteorológico del Área Metropolitana del Valle de Aburrá, Master's thesis, Universidad Nacional de Colombia - Sede Medellín, <http://bdigital.unal.edu.co/54581/>, 2016.

Serra, J.: *Image Analysis and Mathematical Morphology*, Academic Press, Inc., Orlando, FL, USA, 1983.

Sidle, R., Gomi, T., and Tsukamoto, Y.: Discovery of zero-order basins as an important link for progress in hydrogeomorphology, *Hydrological Processes*, pp. 1–7, doi:10.1002/hyp.13246, <http://doi.wiley.com/10.1002/hyp.13246>, 2018.

Sivapalan, M., Takeuchi, K., Franks, S. W., Gupta, V. K., Karambiri, H., Lakshmi, V., Liang, X., McDonnell, J. J., Mendiondo, E. M., O'Connell, P. E., Oki, T., Pomeroy, J. W., Schertzer, D., Uhlenbrook, S., and Zehe,

E.: IAHS Decade on Predictions in Ungauged Basins (PUB), 2003–2012: Shaping an exciting future for the hydrological sciences, *Hydrological Sciences Journal*, 48, 857–880, 2003.

1175 Steiner, M., Houze, R. a., and Yuter, S. E.: Climatological Characterization of Three-Dimensional Storm Structure from Operational Radar and Rain Gauge Data, doi:10.1175/1520-0450(1995)034<1978:CCOTDS>2.0.CO;2, [https://doi.org/10.1175/1520-0450\(1995\)034<1978:CCOTDS>2.0.CO;2](https://doi.org/10.1175/1520-0450(1995)034<1978:CCOTDS>2.0.CO;2), papers3://publication/uuid/D11C9905-6CE2-40B5-8A93-5E5300EB3A6E, 1995.

Takahashi, T.: Debris flow, Taylor y francis, 2 edn., 1991.

1180 Tramblay, Y., Bouaicha, R., Brocca, L., Dorigo, W., Bouvier, C., Camici, S., and Servat, E.: Estimation of antecedent wetness conditions for flood modelling in northern Morocco, *Hydrology and Earth System Sciences*, 16, 4375–4386, doi:10.5194/hess-16-4375-2012, 2012.

Turkington, T., Ettema, J., Van Westen, C. J., and Breinl, K.: Empirical atmospheric thresholds for debris flows and flash floods in the southern French Alps, *Natural Hazards and Earth System Sciences*, 14, 1517–1530, doi:10.5194/nhess-14-1517-2014, 2014.

1185 Vannier, O., Anquetin, S., and Braud, I.: Investigating the role of geology in the hydrological response of Mediterranean catchments prone to flash-floods: Regional modelling study and process understanding, *Journal of Hydrology*, 541, 158–172, doi:10.1016/j.jhydrol.2016.04.001, <http://dx.doi.org/10.1016/j.jhydrol.2016.04.001>, 2016.

1190 Vélez, J.: Desarrollo de un modelo hidrológico conceptual y distribuido orientado a la simulación de crecidas, Tesis doctoral - Universidad Politécnica de Valencia, p. 266, 2001.

Wagener, T., Gupta, H., Yatheendradas, S., Goodrich, D., Unkrich, C., and Schaffner, M.: Understanding sources of uncertainty in flash-flood forecasting for semi-arid regions., IAHS Publication 313, pp. 204–212, 2007.

1195 Wagner, W., Lemoine, G., and Rott, H.: A method for estimating soil moisture from ERS Scatterometer and soil data, *Remote Sensing of Environment*, 70, 191–207, doi:10.1016/S0034-4257(99)00036-X, 1999.

Wu, W. and Sidle, R. C.: and Number Values Agreed Closely With, *Water Resources*, 31, 2097–2110, doi:10.1029/95WR01136, 1995.

1200 Yamanaka, T. and Ma, W.: Runoff prediction in a poorly gauged basin using isotope-calibrated models, *Journal of Hydrology*, 544, 567–574, doi:10.1016/j.jhydrol.2016.12.005, <http://dx.doi.org/10.1016/j.jhydrol.2016.12.005>, 2017.

Yatheendradas, S., Wagener, T., Gupta, H., Unkrich, C., Goodrich, D., Schaffner, M., and Stewart, A.: Understanding uncertainty in distributed flash flood forecasting for semiarid regions, *Water Resources Research*, 44, 1–17, doi:10.1029/2007WR005940, 2008.

1205 Younis, J., Anquetin, S., and Thielen, J.: The benefit of high-resolution operational weather forecasts for flash flood warning, *Hydrology and Earth System Sciences Discussions*, 5, 345–377, doi:10.5194/hessd-5-345-2008, 2008.

Yuter, S. E. and Houze, R. A.: Measurements of Raindrop Size Distributions over the Pacific Warm Pool and Implications for Z–R Relations, *Journal of Applied Meteorology*, 36, 847–867, doi:10.1175/1520-0450(1997)036<0847:MORDO>2.0.CO;2, [https://doi.org/10.1175/1520-0450\(1997\)036<0847:MORDO>2.0.CO;2](https://doi.org/10.1175/1520-0450(1997)036<0847:MORDO>2.0.CO;2), 1997.

Zehe, E., Graeff, T., Morgner, M., Bauer, A., and Bronstert, A.: Plot and field scale soil moisture dynamics and subsurface wetness control on runoff generation in a headwater in the Ore Mountains, *Hydrology and Earth System Sciences*, 14, 873–889, doi:10.5194/hess-14-873-2010, 2010.

1215 Zoccatelli, D., Borga, M., Viglione, A., Chirico, G. B., and Blöschl, G.: Spatial moments of catchment rainfall: Rainfall spatial organisation, basin morphology, and flood response, *Hydrology and Earth System Sciences*, 15, 3767–3783, doi:10.5194/hess-15-3767-2011, 2011.